Intrinsic Optical Imaging of ECM Mechanics

Raphaël Turcotte and Yanhang Zhang

Abstract This chapter provides a comprehensive introduction to optical imaging in the context of extracellular matrix (ECM) mechanics. The goal is to address the critical aspects of optical microscopy so that researchers in the biomechanics research field are able to take full advantage of optical imaging technologies in their studies. Optics is of particular interest to answering questions of multiscale mechanics because of its multiscale nature; information can be obtained at the tissue, fiber, and even molecular levels. Revealing the microstructure of the load-bearing ECM constituents, elastin and collagen, and the interplay between ECM structure and mechanical loading is probably the area where optical microscopy has contributed the most to our understanding of ECM mechanics in recent years. The discussion is therefore confined to optical imaging technologies able to resolve ECM fibers using signals from molecules endogenous to tissue and emphasizes the importance of unbiased imaging and image analysis. Descriptions of polarimetric multiphoton microscopy and adaptive optics are also provided because of their potential for enabling discoveries in ECM mechanics. Although arteries are used here as an exemplar tissue, all concepts covered in this chapter are expected to be generalizable to other organs and tissues.

1 Introduction

Elastic and collagen fibers are the major ECM components in blood vessels (Fig. 1). Elastic fibers endow blood vessels with critical mechanical properties such as flexibility and extensibility. They are essential for accommodating deformations encountered during physiological function of arteries, which undergo repeated cycles of extension and recoil. In the medial layer of elastic arteries, elastic fibers form thick

R. Turcotte (✉)
University of Oxford, Oxford, UK
e-mail: raphael.turcotte@pharm.ox.ac.uk

Y. Zhang
Boston University, Boston, MA, USA

Y. Zhang (ed.), *Multi-scale Extracellular Matrix Mechanics and Mechanobiology*,
Studies in Mechanobiology, Tissue Engineering and Biomaterials 23,
https://doi.org/10.1007/978-3-030-20182-1_6

concentric fenestrated layers of elastic lamella. Together with alternating layers of smooth muscle cells and medial collagen, these elastic lamella form a functional unit of the arterial wall (Fig. 1a–c) [21]. Adventitial collagen, commonly described as a meshwork of helically woven fibers layered around the vessel wall [40], provides structural integrity at higher strains (Fig. 1d).

Determining how the ECM components contribute to the mechanical behavior of an artery is essential for understanding the mechanisms of vascular remodeling and disease progressions. Optical imaging plays an important role in the study of the effect of ECM structural changes on vascular function. Information obtained through improved medical imaging and biomechanical testing methods would be useful in the understanding of vascular remodeling associated with diseases. Several methods, including optical coherence tomography and Brillouin microscopy, can be used to directly measure mechanical properties [45, 75, 79]. Other optical technologies such as point-scanning microscopy and micro-optical coherence tomography are able to provide information about the ECM organization within biological tissue [19, 117]. In particular, the last decade has seen a surge in the application of multiphoton microscopy to ECM mechanics. Multiphoton microscopy enables visualizing the microstructure of the two main ECM constituents, collagen and elastin fibers, in three dimensions (Fig. 1a–d) [80] and imaging in intact tissue, even in living organisms. The ability to image intact tissue is of paramount significance as it implies that imaging can be coupled with mechanical loading (Fig. 1e). The opportunity to

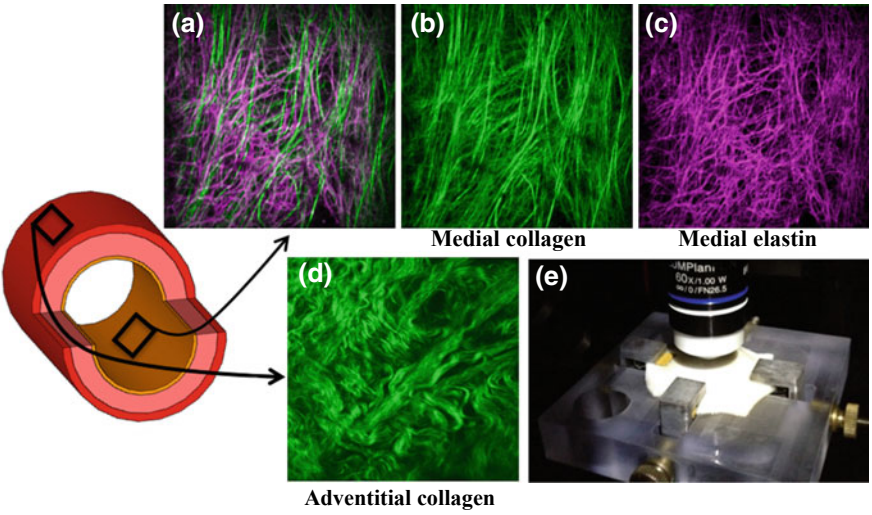

Fig. 1 Optical imaging of ECM in porcine thoracic aorta with multiphoton microscopy. **a–c** Images from the media are shown with **a** both collagen (green) and elastin (magenta), **b** only collagen, and **c** only elastin (image width: 300 μm). **d** Image of collagen from the adventitia (image width: 200 μm). **e** Combining imaging and mechanical loading that allows the sample to be imaged while subjected to biaxial stretching [17]

link the microstructure of elastin and collagen to the tissue mechanical properties provides important insights into the complex multiscale nature of tissue mechanics. The mechanical roles of ECM constituents that cannot be optically measured can also be studied indirectly through their impact on the elastin and collagen fibers microstructure and mechanics [60, 61]. Finally, it is also possible to widen the multiscale window offered by multiphoton microscopy when considering polarization to include the molecular organization of ECM fibers [34, 91].

2 Fundamentals of Optical Imaging

Before diving into a discussion on aspects of imaging directly related to multiscale ECM mechanics, it is necessary to briefly introduce some fundamental concepts of optical imaging. Here, we attempt to provide an intuitive picture sufficient for fully understanding the core ideas of this chapter.

2.1 Optical Images

An optical imaging system is an instrument that uses light to obtain spatially-defined information about a sample [6, 27, 63]. The general working principle of optical imaging is that light is shined onto a sample, altered by the sample through a light-matter interaction, and then detected by a device converting the optical signal to an electrical one. The type of information acquired does not only depend on the light-matter interactions occurring in the sample, but on the nature of the illumination and light-detection systems as well. The strength, or magnitude, of the light-matter interaction being space-variant, the physical parameter containing the desired quantitative information about the sample is usually represented in a structure-preserving map: the *image*.

The above definition of optical imaging is broad, and it aims to encompass the wide variety of existing experimental systems. Essential to the definition of imaging is the fact that a physical property should vary in space; otherwise, the generated uniform image is equivalent to a point measurement. This leads to an alternative definition of (scientific) images that is more closely related to the experimental configuration: a collection of point measurements in an n-dimensional space arranged to conserve the relative dimensional organization. It should be noted that imaging technologies do not perfectly map the object information. For example, the signal at one location may be "contaminated" with signal from other locations [64] or optical aberrations might alter the mapping [27]. Also, different sources of noise can contribute to the imperfect mapping of information in optical images [63].

2.2 Contrast and Spatial Resolution

How much the signal varies between "adjacent" points within the observed volume is often referred to as the *contrast* (or modulation) and is a useful metric to characterize the performance of an imaging system or modality, although it can be dependent on the imaged sample. Contrast is expressed in term of the signal intensity (I) and is quantified as [37]:

$$\mathcal{C} = \frac{I_{max} - I_{min}}{I_{max} + I_{min}} \tag{1}$$

where I_{max} corresponds to the brightest pixel and I_{min} to the dimmest one. It can intuitively be understood as our ability to visualize objects (white), to distinguish them from the background (black, Fig. 2) [7]. The contrast is ideally high and close to its maximal value of 1.

Another metric to characterize the performance of an imaging system, the *spatial resolution,* addresses how the intensity varies spatially (Fig. 3a, b). Here, it is essential to understand that an infinitesimal object will appear to have a larger size in the image (Fig. 3c). Indeed, filtering of the optical signal occurs in such a way that all objects (and borders) will have a minimal size determined by the physical parameters of the microscope. Great importance is (rightfully) placed on spatial resolution because it dictates the length scale of objects that can be resolved with a given microscopy technique. More formally, spatial resolution is commonly defined in two ways: (1) the width of the impulse response of a system (Fig. 3) [63], or (2) the minimal distance required to resolve, or identify the presence of, two adjacent point objects [103]. Each of these two definitions comes with its own criteria on how to quantify resolution. Metrics for characterizing spatial resolution are usually presented as scalars for simplicity. It is nevertheless important to keep in mind that spatial resolution may be anisotropic. Often, the resolution is constant within the imaging plane (lateral axes), but lower in the direction orthogonal to the imaging plane (axial axis) [63].

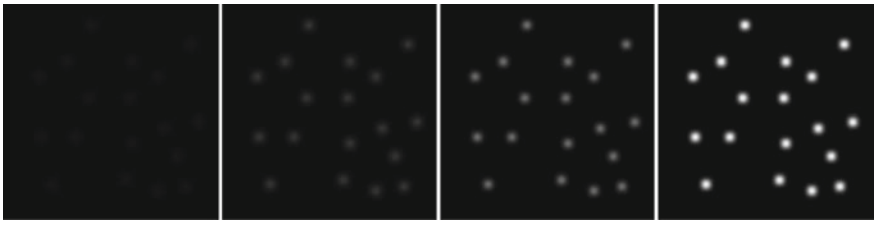

Fig. 2 Contrast. Images of point objects with, from left to right, increasing contrast

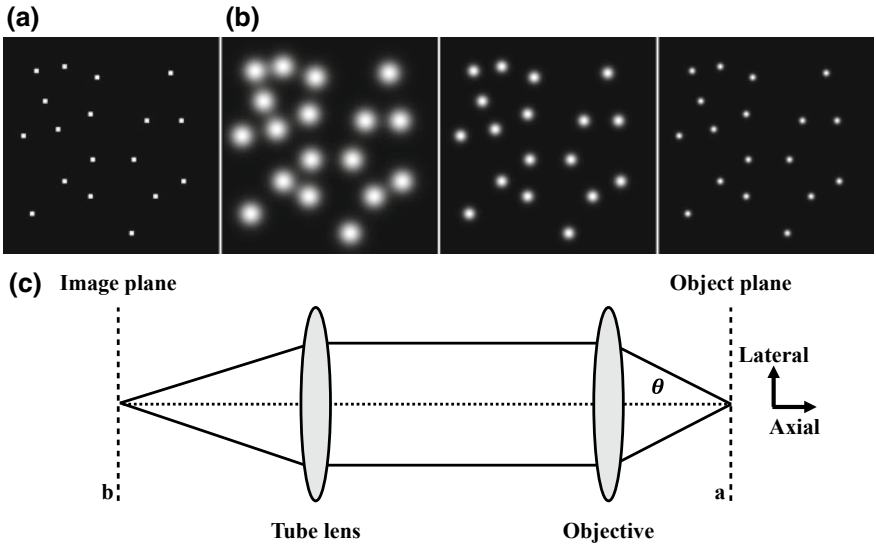

Fig. 3 Spatial resolution. **a** Point objects distribution. **b** Images of point objects with, from left to right, increasing spatial resolution. **c** Schematic of an imaging system

2.3 Temporal Resolution

Resolution can also be temporal. The *temporal resolution* quantifies the minimal time between two sequential images, e.g. the highest achievable imaging rate. It can be limited by the instrumentation because some operations have a finite duration (i.e., a camera takes time to read and send data to a computer). The brightness of the sample must also be considered because enough photons must be detected to obtain an image of sufficient quality and this means that the duration of the illumination period may have to be increased for achieving high contrast in dim samples [65].

When thinking about ECM constituents such as elastin and collagen and their mechanical roles, knowing their spatial arrangement is essential. To determine their microstructure, it is necessary to perform volumetric, or three-dimensional (3D), structural imaging. How long it takes to acquire 3D data is determined by the imaging rate. This parameter will often pose a practical limit on the observable volume fraction (spatial sampling) within an experiment. Imaging can also be dynamic: the same region is imaged repetitively. This would enable, for example, seeing structural changes during viscoelastic relaxation [98]. Dynamic imaging is also necessary for functional imaging where the goal is to measure molecular transients in cells or any other marker of functions. For instance, it might be of relevance to look at calcium transients in smooth muscle cells (functional imaging), when cellular contraction changes the structure of the soft tissue, and describe how the ECM around those cells is changed during a single event (dynamic imaging) [39]. In short, the temporal resolution dictates the time scale of observable processes.

2.4 Summary on Fundamentals of Optical Imaging

Image, contrast, spatial resolution, and temporal resolution are concepts that have to be considered when selecting an imaging modality and system. Contrast and spatial resolution are closely related, but we would argue that they need to be independent to be meaningful. Indeed, some definitions convolute contrast with resolution and some information is then lost about the imaging system. This section was not meant to present the physical principles behind those concepts. For more information on these topics, we recommend reading *Fundamentals of Biomedical Optics* by Caroline Boudoux as its content will be accessible to experts in non-optics fields (including biomechanics) [7]. For a formal introduction to optical microscopy, the reader is directed to *Introduction to Optical Microscopy* by Mertz [63].

3 ECM Imaging Modalities

The development of optical imaging technologies is closely related to their usage in biological applications. Several systems have been applied to visualize the main constituents of the ECM, collagen and elastin, or to measure their mechanical properties [79, 116, 117]. Nowadays, optical microscopes are ubiquitous in research institutions and their operation is becoming more user-friendly. It nevertheless remains essential to understand how signal is being generated and how tissue is altering this signal. In this section, we will present ECM imaging modalities based on different contrast mechanisms, which are light-matter interactions modulating the light field and thus making the contrast, as defined in Eq. 1, non-null.

We will focus our discussion around intrinsic contrast mechanisms. Such mechanisms are defined by the fact that the light-matter interaction takes place with molecules endogenous to the tissue of interest [113]. This is in contrast to exogenous contrast mechanisms which require the introduction of an additional molecule into the sample through some labelling strategies (molecular targeting or genetic modification). Intrinsic, or endogenous, contrast mechanisms possess a series of properties making them advantageous for imaging in the context of ECM mechanics:

1. Issues related to labelling uniformity are avoided. It is important that the detected signal quantitatively represents the distribution (including the concentration) of the molecular species of interest in the tissue. Nonuniformities associated with extrinsic labeling will lead to nonlinearities in the mapping between the sample and the image, thus limiting the usefulness of quantitative information.
2. The signal directly informs on the structure of interest. Directly probing the molecules of interest not only allows accurately mapping structures but also enables characterizing other properties [10]. With exogenous contrast, such measurements, when at all possible, required specialized labeling agents.
3. Tissue processing is not needed. Beyond saving time, the elimination of tissue processing ensures that the tissue's mechanical properties are not altered by the

introduction of exogenous agents forming chemical bonds with the tissue and potentially altering the molecular environment (viscosity, hydration, etc.).
4. Compatible with in vivo (intravital) experiments. Intrinsic imaging techniques developed for excised tissue samples can readily be employed in live animals as no additional sample processing is needed other than the required surgery.

We should note here that the use of exogenous signals also has some important advantages over intrinsic ones. First, specific molecules can be targeted in a fashion that is not dependent on the molecular integrity of the structure of interest. This ability makes it possible to visualize altered ECM constituents in a pathological context. Also, not all ECM constituents can emit light endogenously, but exogenous labels can make them visible. Finally, the signal strength of exogenous agents and their spectral emission bandwidth can be modulated according to experimental needs, resulting in a more flexible system.

3.1 Scattering and Fluorescence Microscopy

In this section, we address **linear, or one-photon, interactions, which occur when one photon interacts with the tissue to generate a different photon**. As photons travel through tissue, they have a probability (termed "cross-section") to interact with molecules. A large portion of the light will be absorbed or diffused by the tissue and will not produce a useful contrast. This absorption and diffusion lead to an exponential decrease of the illumination power as a function of the propagation path length and limits the imaging depth. Other interactions generate a signal suitable for ECM imaging: fluorescence and scattering, both of which can be understood through energy level diagrams (Fig. 4) [7].

Elastin and collagen can both be visualized by fluorescence (Fig. 5) [53, 111]. For fluorescence, a photon is absorbed by a molecule in the ground state $|S_0\rangle$ (Fig. 4a). The photon energy E_{exc} brings the molecule into an excited state $|S_1\rangle$. When the molecule relaxes, on a time scale of nanosecond, a photon of lower energy E_{em}, or equivalently of longer wavelength, is emitted. This wavelength shift between excitation and emission is known as the Stokes shift (Fig. 6a). The Stokes shift originates from the relaxation of vibrational states ν_i, which occurs on a picosecond timescale. The Stokes shift facilitates the spectral separation between the excitation and emission. In the case of elastin and collagen, they can both be excited in the ultra-violet region, with a peak at ~335 nm (Fig. 6a) [94]. Fortunately, elastin undergoes a larger shift than collagen, enabling the spectral separation of their endogenous fluorescence emission [86]. Endogenous fluorescence can also be referred to as autofluorescence. This "self" fluorescence is often considered detrimental in most exogenous fluorescence imaging applications based on extrinsic labels as it can reduce the specificity of the detected signal.

Linear fluorescence can be generated at any location along the light path. Even if the object of interest is properly positioned with respect to the objective lens and its

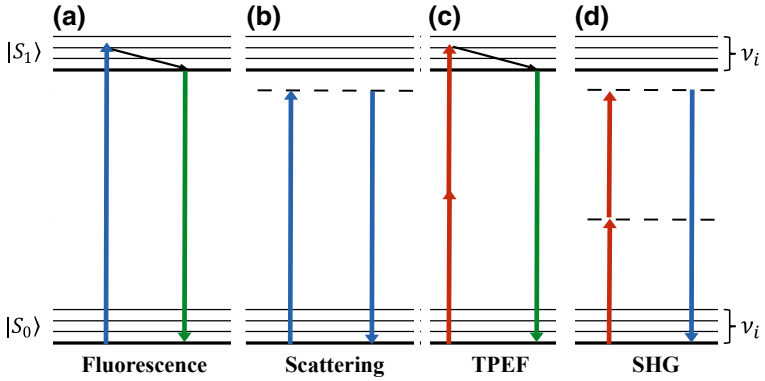

Fig. 4 Energy level diagrams for **a** one-photon fluorescence, **b** linear scattering, **c** two-photon excited fluorescence (TPEF), and **d** second-harmonic generation (SHG). An energy level diagram, also known as a Jablonksi diagram, is a representation of the electronic states for molecule (horizontal lines) and the transition routes between those states (vertical arrows). The ground state $|S_0\rangle$, singlet excited state $|S_1\rangle$, and their related vibrational states ν_i are typically included. Virtual states can also be included (horizontal dashed lines). The vertical axis represents an energy scale. The horizontal axis facilitates the display of event sequences but is not strictly a temporal axis

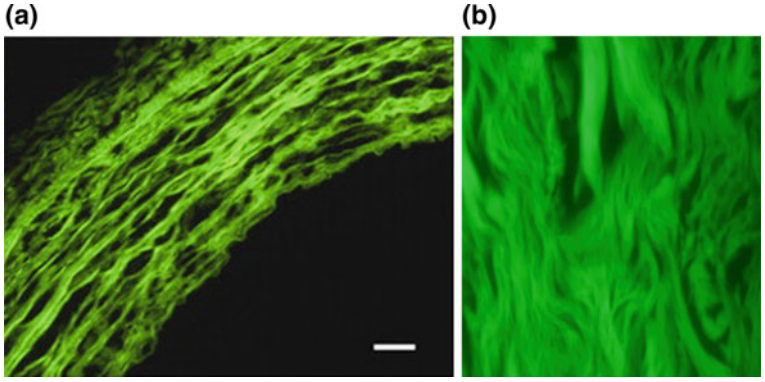

Fig. 5 Linear fluorescence images of **a** elastin in a circumferential cross-section of a porcine carotid artery (scale bar: 50 μm) and **b** collagen in human skin. Reproduced with permission from [53] and [111], respectively

signal correctly transmitted to the optical detector in the image plane, out-of-focus fluorescence from objects located above or below the object plane can contaminate the image [64]. As determining the 3D organization of ECM fibers requires knowing the axial plane from which the signal originate, a strategy for rejection of the out-of-focus signal is needed. Confocal microscopy is a solution to this problem. In confocal microscopy, the illumination light is focused to a single point by the objective and the fluorescence output is filtered in the image plane by a pinhole [70]. The position of the pinhole is such that only the in-focus fluorescence (light from the axial plane

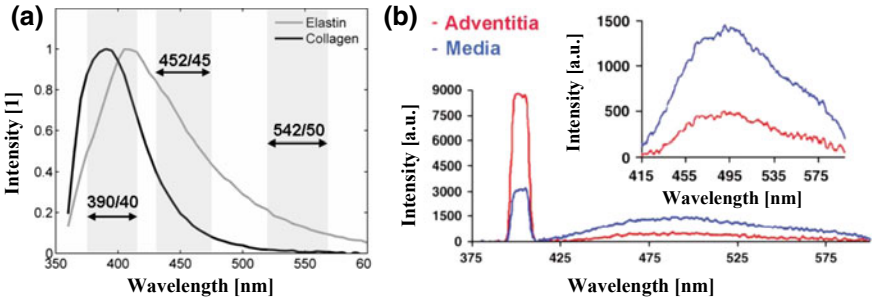

Fig. 6 Emission spectra. **a** One-photon autofluorescence emission spectra from elastin and collagen and three spectral regions (gray, numbers indicate central wavelength/bandwidth) for fiber identification through ratiometric analysis [86]. **b** Combined second-harmonic generation (SHG) and two-photon excited fluorescence (TPEF) from arterial tissue at different excitation wavelength [116]. Reproduced with permission

where the focus occurs in the object, optical sectioning) will go through and reach a point photo-detector (e.g. photomultiplier tube and avalanche photodiode). An image is formed by translating the focal point laterally and sequentially acquire the signal for each pixel. Even when hundreds of thousands of pixels must successively be recorded to form a complete image, the imaging rate can reach 30 frames per second [93].

Achieving optical sectioning is also possible with widefield fluorescence imaging techniques, in which the entire field of view is illuminated at once and the image formed onto a camera. These techniques have in common that (*i*) multiple widefield images need to be acquired with some variation in the illumination pattern and (*ii*) the optically sectioned image is produced in post-processing by combining the multiple raw images. For example, optical sectioning structure illumination microscopy (OS-SIM) requires at least three images recorded with a sinusoidal illumination pattern that is phase shifted between the images [64, 68, 104]. HiLo microscopy requires two images: one with a uniform illumination and a second with non-uniform illumination containing high spatial frequency variations [54, 55]. OS-SIM and HiLo microscopy have not been widely applied to ECM imaging, but would be suitable when a high imaging speed is required. Indeed, although multiple raw images must be acquired to produce a single optically-sectioned image, widefield imaging can reach hundreds and even thousands of frame per second [20, 57, 84].

Scattering is another important light-matter interaction for imaging. During a scattering event, the photon is not absorbed by a molecule, but causes an oscillation of the electronic cloud, which brings the molecule to a virtual state [7]. At the end of the oscillation, a photon of equal energy to the incident one leaves the system, with a different direction (Fig. 4b). The concept of confocal point-scanning microscopy also applies to scattering. Scattering differs from fluorescence in that it doesn't offer chemical specificity, i.e. the signal doesn't originate from a specific molecular component allowing one to distinguish collagen from elastin or any other

scatterers. Instead, a scattering microscope maps variation in the index of refraction and linear scattering has a limited usefulness for ECM imaging because of the lack of specificity. Its nonlinear counterpart is nevertheless important enough for ECM imaging that understanding scattering is relevant.

3.2 Multiphoton Microscopy

Nonlinear, or multiphoton, light-matter interactions occur when two or more photons interact with a material and generate another photon [9]. Two-photon excited fluorescence (TPEF) is the nonlinear counterpart to one-photon fluorescence and occurs when a molecule absorbs two photons simultaneously and reaches an excited state (Fig. 4c) [114]. The following processes of molecular relaxation and emission of a fluorescence photon are then equivalent between linear and nonlinear excitation. Because two photons contribute to the excitation, their energy only needs to be about half of that required for single photon excitation. Therefore, lasers operating at longer wavelengths, in the near infrared between 700 nm and 900 nm, are employed for multiphoton ECM imaging [117]. The use of longer wavelengths increases the penetration depth by reducing the scattering [43, 47], but also by reducing absorption from water and blood [81]. This is a substantial benefit for imaging in thick tissue, especially considering the short linear excitation wavelength of elastin and collagen (<400 nm).

The optimal illumination wavelength for TPEF of elastin is at 730 nm [117]. The emission spectrum is broad with a peak at ~495 nm (Fig. 6b). The large wavelength shift (~80 nm) between the one- and two-photon emission spectra is indicative that different endogenous molecules are at the origin of elastin autofluorescence [100]. Indeed, not all molecules generating a strong linear fluorescence signal will generate an equivalently strong nonlinear signal, and reciprocally, some molecules with a relatively strong nonlinear signal might yield a weak linear fluorescence [23]. In fact, the TPEF from collagen is weak to the point that a different multiphoton contrast mechanism is used to visualize collagen: second-harmonic generation (SHG).

SHG is the nonlinear counterpart to scattering (Fig. 4d) and requires two photons to cause oscillations of the electronic cloud on the same molecule for a single photon at exactly half the wavelength to be produced. The SHG emission spectrum has nonetheless a non-zero width but this width remains very narrow compared to fluorescence (Fig. 6b). The optimal excitation wavelength for SHG from collagen is at 800 nm, which results in an SHG emission at 400 nm [117]. This SHG emission does not overlap with TPEF from elastin, which facilitate the spectral separation of signals in comparison to linear fluorescence. SHG can only occur in non-centrosymmetric media (not possessing an inversion symmetry) [9]. There are few biological structures having permanent dipole moments that are sufficiently ordered and non-centrosymmetric. However, collagen is a highly ordered fibrillar structure and can produce strong SHG which effectively provide signal specificity [11, 14]. As a consequence, SHG was rapidly adopted to image collagen in arteries, skin, tendon,

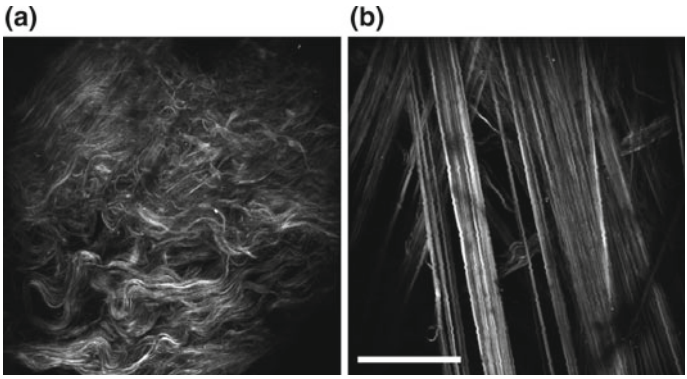

Fig. 7 Multiphoton imaging in porcine aorta. **a**, **b** SHG images from adventitial collagen **a** with no strain and **b** with a 40% strain (scale bar: 180 μm). Reproduced with permission [91]

and other tissues where the ECM plays an important mechanical role [8, 114, 116, 117]. It should be noted that different types of collagen do not generate the same amount of second-harmonic signal. Fibrillar collagen of type I and II produce the strongest SHG signal, whereas non-fibrillar type IV and V provided very limited SHG contrast. Collagen of type III yields weak SHG signal even though it has a fibrillar arrangement [72]. Exemplar images of adventitial collagen in porcine aorta during a mechanical loading experiment are shown in Fig. 7. Of note, the molecular alignment of collagen fibril creates a polarization effect that can be deleterious for structural imaging applications as the signal will be dependent on the fiber orientation in the laboratory frame and the incident polarization [85]. Fortunately, this effect can be alleviated by using a circularly polarized incident light [14].

The probability that two photons arrive at the same location and at the same time, within the extent of the Heisenberg uncertainty principle, is low and thus so is the cross-section for TPEF and SHG [114]. For this reason, multiphoton microscopy is generally implemented with spatially focused excitation (point-scanning) from a pulsed laser source. The use of laser pulses effectively compresses in time the arrival of photons at the focus. These two strategies suffice to generate enough photons for high-quality images to be formed. The requirement for a high photon density for multiphoton events to occur has the benefit that the out-of-focus background is negligible. Optical sectioning is therefore an intrinsic property of multiphoton microscopy (Fig. 8); no confocal pinhole is necessary.

3.3 Summary of ECM Imaging Modalities

In recent years, there have been a very large number of studies in which collagen and elastin were imaged with SHG and TPEF microscopy, respectively, to study the

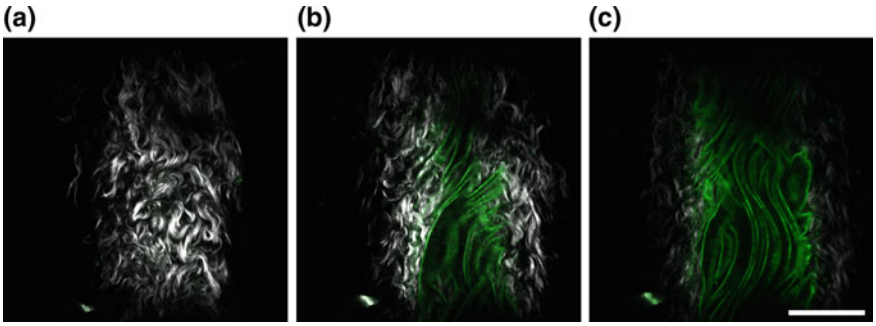

Fig. 8 Multiphoton imaging in murine carotid artery. Images at different depths showing **a** adventitial collagen, **b** the transition between adventitial and medial layers, and **c** medial elastin (TPEF: green; SHG: white; scale bar: 100 μm). Reproduced with permission from [108]

relation between tissue mechanics and microstructure. Constitutive modeling of soft biological tissue is a challenging field of research due to the complexity of the tissue behavior, hierarchical structures in the tissue, and the ability of biological tissue to remodel in response to stimuli. Advances in optical methods and image processing techniques have made possible exploring/quantifying the architecture of ECM structural components of soft tissues at different scales. Using multiphoton microscopy, arterial elastin and collagen has been simultaneously captured in previous studies [16, 17, 26, 110]. Constitutive formulations that are motivated by the tissue structure has been proposed for biological tissues, along with many studies attempted to incorporate some of the structural information into the structural-based constitutive models [38, 95, 99, 109, 110]. In sum, SHG and TPEF are powerful modalities for ECM imaging because intrinsic signals are available to visualize collagen and elastin, respectively, in 3D at a length-scale appropriate for mapping the fiber microstructure.

4 Prospective ECM Imaging Technologies

This chapter on optical imaging of the ECM would not be complete without discussing more advanced technologies. Some of these technologies can be implemented as add-ons to standard microscopes. Beyond instrumentation, advanced imaging techniques can also refer to the status of the sample. In this section, we will cover the following technologies: polarimetric multiphoton microscopy and adaptive optics. These technologies have yet to be exploited to their full potential to study ECM mechanics.

4.1 Polarimetric Multiphoton Microscopy of ECM Molecular Order

So far, we have focused on techniques quantifying intensity, not phase or polarization. Intensity provides information on the microscopic scale and is ideal to map the microarchitecture of the ECM. The multiscale relation between microstructure and tissue mechanics can be extended to also include molecular organization of ECM fibers. The molecular order can be probed by polarimetric multiphoton microscopy [14, 25, 69, 85]. This technique is particularly relevant for SHG collagen imaging applications, but the appropriate extrinsic labelling agent could enable similar measurements for elastin [10, 52].

At the core of polarimetric multiphoton microscopy is a *polarization dependence* effect. The polarization dependence describes the modulation of the detected (SHG) intensity as a function of the 3D angular relation between the molecular dipole axis of scatterers and the spatial orientation of the electric field oscillation of the illumination light. This dependence can be mathematically expressed by a tensorial quantity, the nonlinear susceptibility [9]. By controlling the polarization of the incident light, it is therefore possible to interrogate the molecular dipole arrangement by determining the nonlinear susceptibility tensor or related quantities.

Polarimetric multiphoton microscopy is usually performed with linearly polarized light, for which the electric field oscillates within a single plane. For collagen fibers residing in the object plane, the SHG intensity will vary as a function of the polar angle between the polarization axis and average molecular orientation within each focal volume (Fig. 9a). By recording multiple images with different orientation of the incident linear polarization, the polarization dependence of the SHG signal can be plotted and fitted to an analytical expression having nonlinear susceptibility tensor elements as free parameters (Fig. 9b). The exact form of the analytical expression depends on the sample and typically involves many geometrical and symmetry assumptions [3, 18]. The intensity variation is large for ECM collagen fibers as they have a highly symmetric molecular structure. If the molecular dipoles had a random distribution, their average orientation would be isotropic and there would be no polarization dependence.

By performing the fitting at every pixel in the image, it is possible to produce maps of the nonlinear susceptibility tensor components (Fig. 10a, b) [13, 18, 62]. These are particularly useful as they show differential molecular organization, which may not be visible with intensity measurements alone or by analyzing intensity variations for the entire image. The existence of different types of collagen is further evidence by the bimodality of the tensor element histogram (Fig. 10c, d).

Several other optical properties related to polarization can be mapped in this way. Of particular relevance for ECM mechanics is the mapping of the principal orientation per pixels [89]. This mapping is spatially more resolved than the results from FFT analysis, as the results from the latter depends on surrounding pixels, whereas adjacent pixels are independent in the polarization analysis.

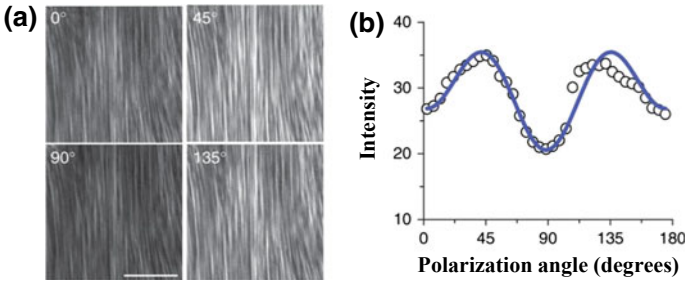

Fig. 9 Polarization dependence. **a** SHG images of collagen recorded at one location with different orientation of the incident linear polarization (scale bar: 50 μm). **b** Plot of the SHG intensity as a function of the polarization angle. Reproduced with permission from [14]

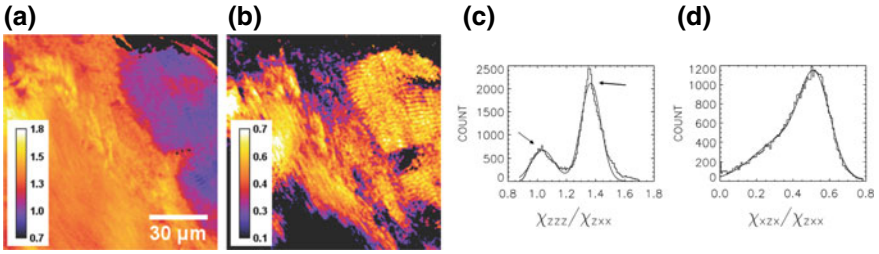

Fig. 10 Molecular imaging at a tendon-muscle junction. **a**, **b** Nonlinear susceptibility tensor element χ_{ijk} ratio mapping of **a** χ_{zzz}/χ_{zxx} and **b** χ_{xzx}/χ_{zxx}. **c**, **d** Histogram distribution of the tensor ratio **c** χ_{zzz}/χ_{zxx} and **d** χ_{xzx}/χ_{zxx} fitted with the sum of two Gaussian functions. Reproduced with permission from [13]

It was mentioned in Sect. 3.2 that the use of a circularly polarized illumination alleviated the effect of polarization dependence and that this was essential for structural imaging of collagen with SHG. It should nevertheless be noted that the nonlinear susceptibility tensor can be characterized using circularly polarized light [24] and that there is a distinction between an image taken with circularly polarized light and an image of the amplitude calculated from fitting the analytical expression for polarization dependence [91].

Polarimetric multiphoton microscopy has been used extensively to study the properties of collagen, but often not enough consideration was given to how the mechanical state of the tissue can affect the measurement. Reciprocally, very few studies have taken advantage of the additional length-scale provide by polarization analysis and this approach has yet to provide new insight into the biomechanics of the ECM. It is expected that as fibers are being recruited to carry a load their molecular organization will change to become more uniformly aligned. Consequentially, the SHG signal measured with circular polarization should increase and the intensity modulation form the polarization dependence should be more pronounced (Fig. 11a, b). Two studies have reported preliminary observation supporting these predictions. The first study reported changes in the SHG signal from adventitial collagen during equal

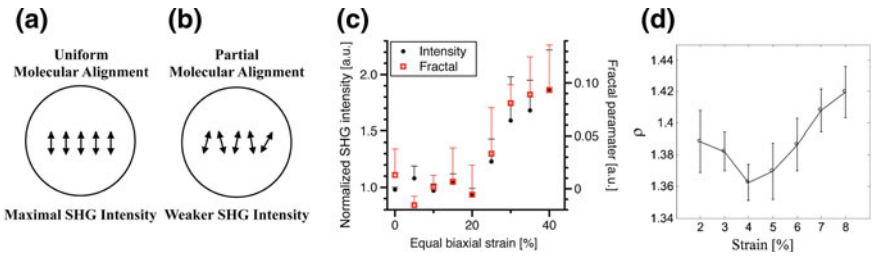

Fig. 11 Molecular ECM mechanics. **a**, **b** The SHG intensity is dependent on molecular alignment for any incident polarization state [91]. **c** Fractal analysis and polarization-dependent intensity measurements during equal biaxial loading of SHG images from adventitial porcine aorta [91]. **d** Optical parameters ρ from rat-tendon obtained from polarization SHG data as a function of strain [34]. Reproduced with permission

biaxial loading in porcine aorta and was measured with circularly polarized light. The observed variation corresponded closely with previous results obtained from fractal analysis—a measure of the degree of self-similarity of an image at different scales. Here changes in the fibrous network was quantified with a parameter corresponding to the normalized variation in fractal number to the initial experimental condition—(Fig. 11c) [91]. A second study characterized different optical parameters in rat tail tendon under mechanical loading [34]. In particular, it is shown how the anisotropy, a parameter related to the nonlinear susceptibility tensor, varies with strain (Fig. 11d), but the authors link this result to fibril orientation. Much remains to be done to link the molecular information to the fiber and tissue levels in order to yield new insight into the multiscale ECM mechanics.

Several factors contribute to the alteration of the polarization state during propagation in biological tissue: birefringence [32, 33], geometrical parameters [88], and scattering [22]. They will not be discussed in detail, but it should be understood that polarimetric multiphoton microscopy is challenging to perform at depth and will often require empirical corrections in order to be accurate. Another important limitation comes from the fact that the structure to be probed does not necessarily lies in the imaging plane, i.e. the azimuthal angle between the linear polarization and the fiber orientation may not be zero. In such common cases, a complete characterization of the nonlinear susceptibility tensor would require probing with axially oscillating polarization states, which requires more advanced optical tools to be generated.

4.2 Adaptive Optics

To assess the mechanical properties of the ECM, it is necessary to image the ECM constituents in situ as they interact together microscopically to give tissue level properties. This multiscale shift precludes relevant mechanical and microstructural information from being obtained by imaging in thin tissue sections or along cuts made

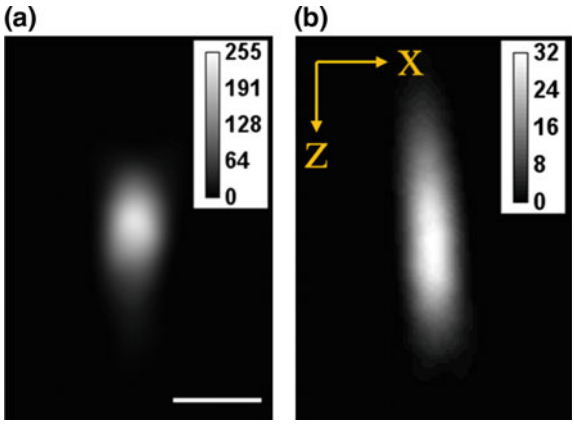

Fig. 12 Optical aberrations. Two-photon fluorescence excitation volume **a** without and **b** with optical aberrations introduced by a tilted glass surface (X: lateral; Z: axial; scale bar: 2 μm). Reproduced with permission from [90]

on excise volumes. As previously mentioned, imaging deep in biological tissue is limited by absorption and scattering, which cause an exponential attenuation of the illumination power. The imaging depth is further decreased by optical aberrations. Optical aberrations are characterized by an alteration of the illumination wavefront,[1] which results in an intensity and spatial resolution losses (Fig. 12) [4, 44]. Therefore, not only is the imaging depth reduced, but the image quality at the accessible depths is degraded. Optical aberrations caused by the sample can have multiple origins. They can originate from a mismatch in index of refraction between the immersion milieu for the optics and the sample [5]. They can also arise from the interface between the sample and immersion milieu being tilted [90] or curved [59]. These situations will result in wavefronts with predictable conformation such as spherical and comatic aberrations.

More challenging to predict are the aberrations generated by the heterogenous index of refraction distribution in biological tissue. Indeed, biological tissues do not, in general, possess uniform optical properties and this can have severe effects on image quality. Methods for wavefront control are therefore needed. Adaptive optics refers to a group of technologies for wavefront control [4, 44]. As there exists many variations in implementation of adaptive optics, we will not review them here. Instead, the two core principles, common to all adaptive optics methods, will be presented: sensing and correction. Sensing refers to the determination of the aberrated wavefront. The measurement of aberrations can either be performed directly or indirectly. Direct wavefront sensing involves measuring the wavefront itself and requires additional optical components to be integrated into the imaging system [2, 96, 97]. In general, direct wavefront sensing has the advantage of being fast, as only a single measurement is needed, but has the disadvantages of having increased instru-

[1] A wavefront is a surface orthogonal to the local propagation vectors on which the phase of the light wave is uniform. For a plane wave, aberrations are causing the wavefront to no longer reside in a single plane, but instead to form a complex 3D surface, i.e. the phases in the plane are not uniform.

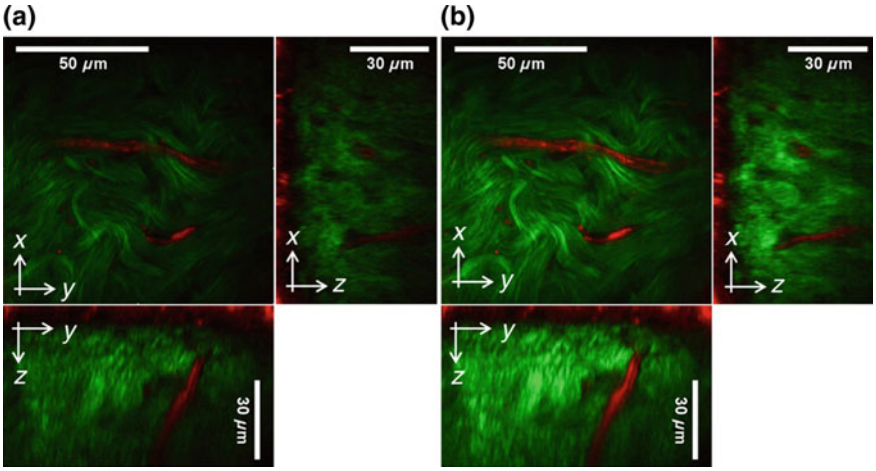

Fig. 13 Adaptive optics. Ex vivo murine skin images (xy) and axial-lateral reconstructions (xz and yz) **a** without and **b** with aberration correction. Green: SHG from collagen. Reproduced with permission from [67]

mental complexity and requiring calibration procedures to be routinely performed for performance to be maintained.

Indirect sensing methods do not directly measure the wavefront, but instead use the signal of interest, either in the form of a point or as an image, as a beacon for an optimization procedure. For instance, the optimization could aim at increasing the contrast in an image or the brightness of a point. In opposition to direct sensing, indirect sensing requires a large number of measurements and is thus slower [44]. It possesses the advantage of not necessitating modification of the microscope, the standard imaging detector being a sufficient sensor. The selection between indirect and direct sensing should therefore be based on a comparison between time constraints (which are likely low for structural ECM imaging) and the availability of support to operate more advanced imaging systems.

Correction of the aberrations is done following a single approach for multiphoton imaging: pre-compensation. The pre-compensation consists in imparting to an unaberrated incident wavefront the same amplitude of phase error as will be encountered in the sample but of the opposite sign. As the shaped wavefront travels through the tissue, the pre-compensation will cancel out the effect of tissue-induced aberrations. Wavefront shaping is achieved by positioning a segmented device which can control the local slopes within a wavefront (either a deformable mirror or a liquid-crystal spatial light modulator) in the appropriate Fourier-conjugate plane. Adaptive optics has been implemented most frequently in bio-imaging for neuroscience applications using multiphoton point-scanning fluorescence microscopy [44], but a few examples of collagen imaging with SHG can be found (Fig. 13) [67].

Increasing the imaging depth and improving image quality with adaptive optics would benefit all ECM imaging applications, but some would profit more from wave-

front control methods than others. Mouse arteries are sufficiently thin to be imaged through their entire thickness with multiphoton microscopy. Unfortunately, their large curvature on the scale of the wavefront from their cylindrical shapes generate a substantial amount of aberrations, making it challenging to visualize medial elastin and to reconstruct elastic lamellae [107]. Collagen bundles in the adventitial layers are also highly aberrating and cause underlying structures to appear dim and smeared (Fig. 22). As will be further discussed, the local shadowing effect from collagen bundles can make quantitative analysis challenging. Unlike the undesirable effect from tissue curvature, collagen bundles cause aberrations that are likely spatially-variant within the field-of-view and are consequentially more challenging to correct. Most current adaptive optics methods are suitable exclusively for spatially-invariant optical aberrations.

4.3 Other Prospective ECM Imaging Technologies

In this chapter, we focus on only two technologies (polarimetric multiphoton microscopy and adaptive optics) to preserve generality. Several other approaches, such as super-resolution imaging, expansion microscopy, and optical clearing, could potentially advance the field of ECM mechanics as well. We will mention them here briefly. Super-resolution microscopy has been demonstrated for ECM imaging in the brain [92]. Its main benefit is the extended spatial resolution it provides, going beyond the diffraction-limit, which could enable detailed mapping of individual fibers in a complex meshwork [78]. Increased spatial resolution is also achieved with expansion microscopy by chemically processing the sample for it to be physically and homomorphically expanded [12]. Unlike super-resolution imaging, this approach is not compatible with mechanical testing, but provides increased light penetration depth by making the sample more transparent. In optical clearing methods, the chemical treatment exclusively aims to make the sample optically transparent without expansion. Here again the goal is to increase the imaging depth and this method has been used together with SHG to visualize skeletal muscle [71].

5 Unbiased Imaging

It is often tempting to immediately place a sample under the microscope and acquire images. Before doing so, there is nevertheless a critical, yet oft-omitted step: designing the imaging study. Even imaging experts will frequently not perform an imaging study and instead report a proof-of-principle that a certain measurement can be performed with their latest device. Unfortunately, this is insufficient to answer questions of ECM mechanics. More likely is that imaging at many (but not all) locations in several samples will be necessary. Going beyond making single measurements is essential but establishing the optimal sampling strategy is not trivial. In this section, we will explore how to think about sample and sampling in the context of ECM mechanics.

5.1 Stereology for Biomechanics

Stereology is the science of analyzing 3D materials such as biological tissue from spatially sampled data [66, 77, 101]. The goal of stereology can be understood as creating a set of approaches and tools to evaluate quantitative parameters—volume, surface area, length, and number, which will be referred to as the first-order stereological parameters—for a sample, and the population it belongs to, when only a fraction of the sample is probed [66]. Stereology can thus be divided into two parts: sampling and analysis. Here, we will look at the sampling; the analysis will be addressed in a later section.

Historically, the spatial sampling consisted of discontinuous cross-sections from fixed and cut tissue because it was not possible to image and analyze the entirety of a sample volume [101]. When imaging is discontinuous, it is not possible to determine with certainty the structures located between two adjacent planes [66]. The main challenge therefore involved extending the information obtained from 2D planes to the full 3D tissue. This extension is not as simple as one might think and failure to account for the difference in dimensionality leads to significant inaccuracies and imprecisions. Most early stereological tools are related to the "2D-to-3D" correspondence and therefore suitable for optical imaging data, which is often intrinsically 2D.

Thanks to advances in automation and imaging speed, it is now common to image samples continuously along the light propagation axis. For the imaging to be continuous implies that the axial sampling is sufficiently high with respect to the spatial resolution such that the volumetric information can be reconstructed between adjacent planes; the uncertainty about structures in between planes is eliminated. As previously mentioned, performing volumetric imaging is critical when assessing the organization of ECM structure, which are located in multiple axial planes due to their waviness, their bundle arrangement, and the tissue curvature. For instance, medial elastic lamellae in mouse carotid arteries might appear as large wavy fibers under two-photon fluorescence microscopy if the axial sampling is not sufficient (Fig. 8b, c), whereas a volumetric reconstruction will reveal its lamellar nature [107]. Volumetric reconstructions are also necessary when assessing relations between two objects, such as the distance between two elastic lamellae. Even if a lamella rests exactly in a single imaging plane, tissue deformation will change the absolute position of this plane with respect to the imaging device such that under some mechanical conditions the lamella might no longer be visible if the axial sampling (the distance between two imaging planes) is insufficient.

For smaller vessels, it is possible that nearly the full thickness can be imaged from the adventitial side (Fig. 14b). For larger vessels, the entire thickness of the sample is rarely imaged (Fig. 14a). The reasons for this are two-fold. First, light is scattered as it propagates through tissue, thus posing a limitation on the imaging depth (as discussed in Sect. 3.1). Second, it is more efficient to keep in line with the stereological perspective, using several 3D sub-volumes distributed throughout a sample to probe the 3D structure of the whole sample. However, in tissues that are thick in comparison to the optical penetration depth, the number of accessible

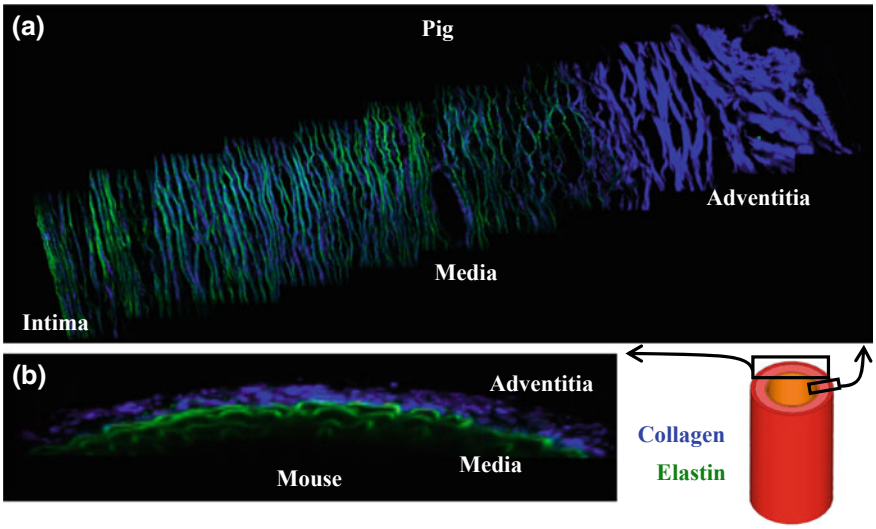

Fig. 14 Multiphoton images of collagen (blue) and elastin (green) acquired in **a** a circumferential cross-section from a pig aorta (width: ~1200 μm) and **b** an intact mouse carotid artery reconstructed to show a circumferential cross-section view (width: 350 μm)

sub-volumes is limited. It is thus questionable whether the ECM structure obtained from a small depth is representative of the ECM network structure in the arterial wall. Transmural variation in elastin fiber distribution was demonstrated by acquiring images from 3D slabs across the thickness (Fig. 15) [108]. It was concluded that the transmural variation in fiber orientation distribution is important in characterizing the anisotropic mechanical behavior of ECM network and should be considered in constitutive modeling of tissue mechanics.

An important question is "how much of the tissue should be sampled?" To answer this question, we should be reminded that the goal of most scientific measurements is to test the information that will be obtained against a multitude of hypotheses and for the conclusions to be extrapolatable to a population. In order to achieve this, it is not only necessary to accurately determine the value of stereological parameters, but also their variation. Therefore, a sufficient fraction of the tissue should be imaged such that this fraction encompasses most of the biological variation in a parameter within a sample, most of the intra-sample biological heterogeneity. A corollary is that enough samples should also be imaged to assess the inter-sample variability. Quantification of both the intra- and inter-sample biological variations are essential. Imaging a large number of samples but only at one location will yield inaccurate and imprecise data. Imaging a single sample in its entirety doesn't provide information about the population it belongs to. In brief, stereology dictates rule which guarantee that spatially sampled imaging data is suitable for statistical inferences [66].

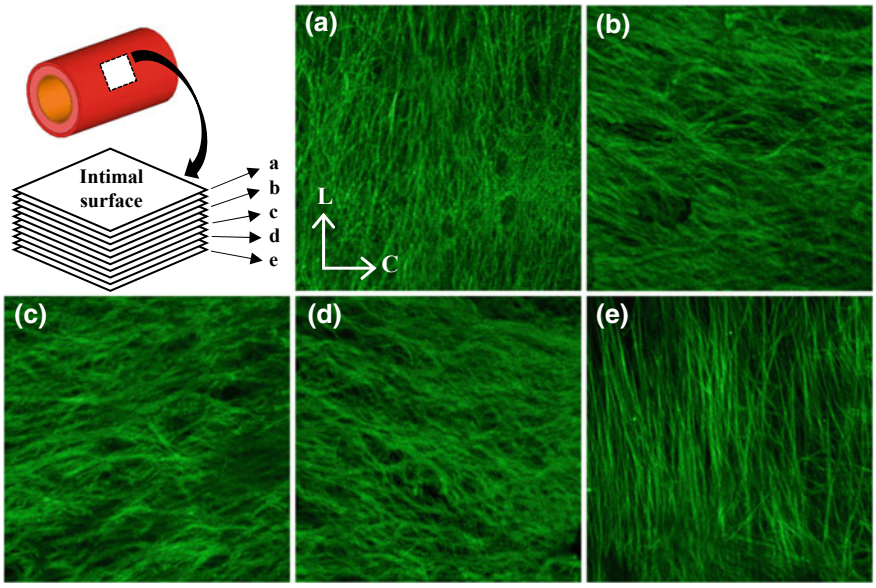

Fig. 15 Multiphoton images showing the distribution of elastin fibers in **a** the inner media, **b**–**d** middle media, and **e** outer media. Images width 250 μm; L: longitude; and C: circumference. Adapted from [108]

5.2 Reference Space

In order to compare different samples, it is essential that the probed regions be consistent. Otherwise the accuracy of the subsequent analysis may be worsened, and the inter-sample variation will be increased. It will then be impossible to separate the variation due to this sampling error and the real biological variation, thus limiting the performance and adequacy of statistical inference methods [42]. It is well known that the content and architecture of elastin and collagen and, hence, the mechanics of aorta vary with anatomical locations throughout the aortic tree [29, 46, 51, 74, 76, 115]. For instance, elastin content [15, 35, 36, 82] and the number of lamellar units [83, 105] appear to drop markedly from proximal thoracic to distal regions of aorta. Therefore, it is essential to establish a *reference space* that can be consistently imaged in different subjects [66].

The structure of the ECM largely dictates the properties of the organs and tissues in which they are located. The goal of imaging in this context is to inform the relation between the ECM and tissue mechanical properties. Consequentially, the reference space should be defined in a way that reflects biological functions [66]. Ideally, the borders of the reference space will correspond exactly with the borders of an organ or biological structure. This definition of the reference space is the most robust one for repeatability. It also enables normalization of volumes to create standardized tissue maps. In addition, volumetric changes/alterations due to growth and remodeling are

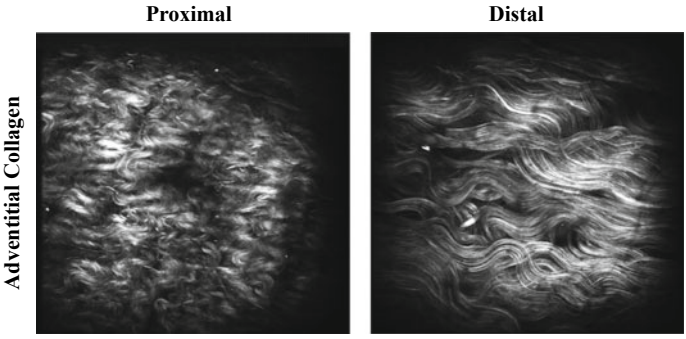

Fig. 16 Representative SHG images of collagen in adventitial collagen of proximal (left) and distal (right) regions of thoracic aortas. Adventitial collagen fibers are highly undulated in the proximal region compared to the distal region while there is no obvious difference in medial elastin and collagen waviness between proximal and distal region (Images width: 360 μm)

common when comparing experimental groups of different age, gender, strain, or disease status, and this definition also allows for correction of these biases.

In large organs, taking a fraction (a sub-region) of a biological structure as the reference space may be beneficial. This is particularly true when results can be sample-matched between ECM imaging and mechanical testing, i.e. the same sample is used for both measurements. The requirement for the reference space to be deterministic remains regardless of the fact that it does not incorporate an entire function or structural biological unit. Indeed, if cuts are made in a tissue, such cuts should be made at morphologically defined positions, and a unique position should be used for a study. For example, the ECM microstructures was found to vary longitudinally in porcine aorta, in accordance to an equivalent mechanical variation (Fig. 16), and such gradient could not have been observed with a random selection of samples within aortas [110]. More importantly, such gradient would generate undesirable inter-sample variation and potentially mask subtle biomechanical phenomena. This illustrates the benefit of using sub-regions as reference space.

We will conclude the discussion on reference spaces by distinguishing them from regions of interest (ROIs). While reference spaces are deterministic, ROIs will only be selected after the imaging and according to the distribution of interesting features within the dataset. The goal of selecting ROIs is to identify groups of pixels on which further analysis should be performed, which contrast with the physiological nature of reference spaces. It is usually challenging to establish formal criteria to define ROIs. As a consequence, it is frequent for different individuals to obtain different quantitative results. Nonetheless, the same qualitative observations should be made. Otherwise, it might be that the ROIs were poorly chosen.

5.3 Systematic Random Sampling

Once the reference space is defined, the next step consists in establishing how it will be sampled. In order to make such a determination two questions must be answered: (1) what fraction of the volume should be imaged and (2) how should the probes (imaging area) be spatially distributed? The volume fraction that should be imaged is determined by the intra-sample variation. The aim is to image enough of the sample to capture its biological heterogeneity. Of course, if the entire sample is imaged, the variance of the imaged volume fraction will correspond exactly to the variance of the sample. However, acquiring such a large amount of data is often technically unrealistic. In the study of ECM mechanics, it is often more informative to image a sample under a number of mechanical conditions. We routinely determine properties of the ECM in porcine aorta by imaging only 10% of the optically accessible volume fraction [17, 60].

The optimal volume fraction can be found by performing a pilot study [1, 66, 102]. This pilot study would consist in imaging a large fraction of a single sample and evaluate the statistical estimates for different volume fractions artificially generated in post-processing. By plotting the statistical estimates as a function of volume fraction, one can then find the smallest volume fraction at which the statistical estimates have converged to the sample values. As independence is needed between samples for statistical inference, the decision of including the sample in which the pilot study was conducted should be taken carefully; independence is lost if a sample included in the experimental group affects the selection of the other samples.

The spatial distribution of the imaging areas should be random for the imaging and sequential quantitative analysis to be unbiased. It is indeed essential for the reference space to be probed randomly for the results to be unbiased. One would correctly expect a non-random and random distribution to appear as shown in Figs. 17a and b, respectively. The reason Fig. 17a represents a non-random probe distribution is because the reference space in partially probed, not because of the systematic arrangement of the probes. It is indeed the case that a partial sampling of the reference space is necessarily not random, as exemplified in Fig. 17c. In fact, the distribution in Fig. 17a is a limiting case of the one in Fig. 17c, where 100% of the partial reference space is probed.

Optimal probe distributions for ECM imaging are shown in Fig. 18 [31]. Two key features are apparent: the probes have a uniform distribution and the distribution is based on the geometry of the reference space. Unbiased stereology requires that no mathematical models be used to inform the probe distribution and that no assumptions be made about the geometry of the reference space [66], the rationale being that biological objects do not follow geometrical rules, and the assumptions and models are thus imperfect. The distributions shown in Fig. 18 are termed *systematic random sampling* if the origin is randomly assigned and the spacing between probes is uniform (systematic) and preserved from sample to sample [31]. The systematic arrangement of probes does not affect the randomness as long as the starting point is randomly assigned for each sample. In previous studies, we performed such assign-

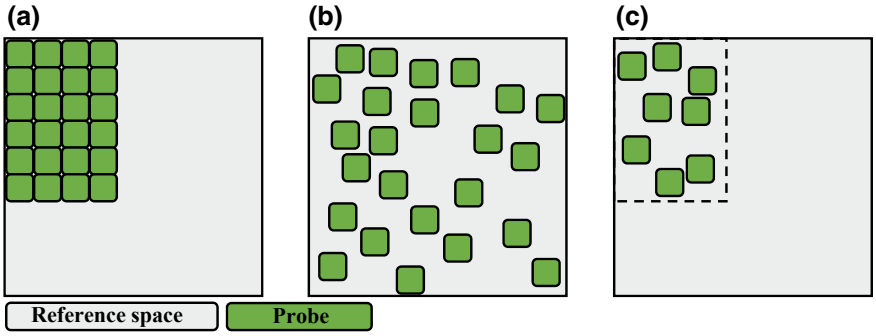

Fig. 17 Sampling distributions. **a** Non-random probe distribution. **b** Random probe distribution. **c** Partial covering of the reference space; non-random probe distribution

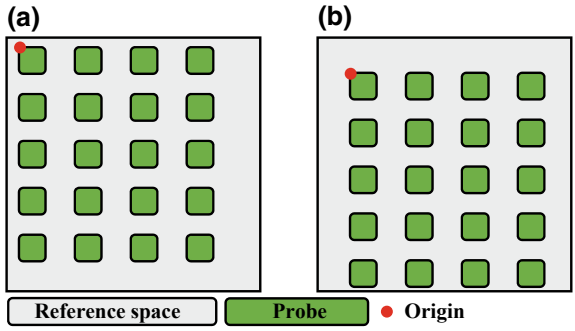

Fig. 18 Systematic random sampling. **a** Equidistant probe separation forms a systematic sampling. The origin must be determined randomly. **b** The same distribution is used for different samples but the origin is randomly changed

ment by arbitrarily positioning the samples, and thus the reference space, under the microscope. Another option would have been to position each sample very exactly under the microscope and use computer generated origin coordinates for each sample. Systematic sampling possesses the important advantage of being more efficient than non-systematic sampling [66]. Less data is required with systematic than non-systematic sampling for the sample estimates to converge. In addition, the uniform spacing makes the data easier to acquire manually or through automation. It should nonetheless be noted that systematic and non-systematic random sampling will provide data of equivalent accuracy.

5.4 Other Experimental Considerations

The last step before beginning data acquisition is to determine a key experimental parameter, the illumination power. The illumination power is the number of photons per unit of time (in watts) incident onto the specimen. For most biological applications, it is desirable to keep this power low because too much light may cause dam-

age, thus altering the biology of interest, and engender photobleaching, a decrease of the signal due to the inability of molecules to be excited multiple times. Collagen and elastin are less vulnerable to photodamage than cells and minimally susceptible to photobleaching [10, 30, 41, 48]. These properties allow for large illumination powers to be used for ECM imaging, although one should be mindful of collagen cross-linking; collagen cross-linking can alter the mechanical properties of the sample and spectrally contaminate the multiphoton fluorescence signal of elastin with new fluorescence signal from collagen [50, 73]. No absolute power values are given here because photobleaching, photodamage, and collagen cross-linking depend not only on the illumination power, but also on other physical parameters such as pixel dwell time and imaging rate.

Using a large illumination power has several advantages. First, it will improve the image quality by increasing the signal-to-noise ratio. Another way of increasing the signal-to-noise ratio consists in acquiring multiple images sequentially and averaging them, which requires more time but is nonetheless advisable (averaging just a few frames can substantially improve image quality). Second, a larger dynamic range is made available, making features which are less bright visible. Third, the imaging depth is increased. The effective illumination power decreases exponentially through tissue due to absorption and scattering, thus limiting the depth at which imaging can be performed. In the past, our strategy has been to find the saturation point at the surface of the samples and use a fixed laser power. Alternatively, the power could be increased to compensate for the attenuation. Adjusting the power of the light source can usually easily be done either through software control or by rotating a wave plate located in front of a prism. In any case, the power should be measured directly with a power meter calibrated for the wavelengths and power range of the source, kept constant for all samples, and saturation absolutely avoided. Due to inter-sample variation in optical properties, it is possible that there will be saturation appearing between the preliminary and main studies or between samples within the main study. It is therefore a good practice to sacrifice some dynamic range by decreasing the laser power by a few percent to avoid saturation. The illumination power should always be reported in scientific publications, as should the reference space and sampling parameters.

5.5 Unbiased Imaging Summary

By performing systematic random sampling of the reference space in a sufficiently large number of samples, a dataset will be generated that is suited for statistical inference. Abiding by stereological rules also means that the experiment will not have to be repeated and can serve as a reference. For instance, we conducted an imaging study of the ECM in porcine aorta to characterize the engagement of collagen and elastin during mechanical loading [17]. Because of the use of unbiased imaging, we were able to use the same data as a baseline to assess the specific role of glycosaminoglycans [60]. Of course, only the imaging strategies is unbiased. A

different set of considerations might be necessary to make the mechanical testing more quantitatively robust. Finally, we would like to note that the terminology used and the selection of concepts to be introduced was based on *Principles and practices of unbiased stereology* by Mouton [66]. Readers should nevertheless note that we depart significantly from the content of that book.

6 Methods for Image Analysis

Image analysis is an important part of imaging, as is the accompanying post-processing. There certainly are many valid ways of analyzing a single dataset, and ideally, each of these should bring us to the same conclusion. Therefore, guidelines for image analysis and reporting of imaging data are presented here that can be generalizable to any chosen analysis method. Quantitative analysis will also be placed into a stereological context. For ECM imaging, it is important to characterize the complex networks at different structural hierarchies; an emphasis will thus be put on how to describe geometric objects in biological tissue efficiently and accurately.

6.1 Standard Approach for Image Analysis

6.1.1 Quantitative Image Analysis

When deploying an imaging modality for a new application, such as imaging an organ from a new experimental animal model, the first step of image analysis should consist in verifying that the optical signal originates from the structure of interest. For example, in early imaging of elastin in the descending aorta of mice, multiphoton fluorescence images were presented with images from histological methods (Fig. 19). It is quite striking in Fig. 19b which elastic lamellae is different from the others, and one might be tempted to stop the analysis at this point. We argue here that imaging analysis should always be *quantitative*, even if the interpretation of the results will be qualitative. Unbiased quantitative analysis is necessary for meaningful reporting of conclusions from statistical inference testing, i.e. significance of the observation should be demonstrated.

Quantifying the imaging data will also help to select the images to display for reporting. Displayed images should be *representative* of the populations studied. An unbiased way of performing this selection is to systematically pick the image for which the quantitative metric is the closest to the average value of the sample. For instance, the image in Fig. 19b of the experimental condition in transgenic (KO) mice should have a "fiber dispersion" value close to 34° as suggested by Fig. 19c. Of course, displaying extreme cases would be more evocative and may thus facilitate the communication of the results, which is an aspect that should not be neglected. It

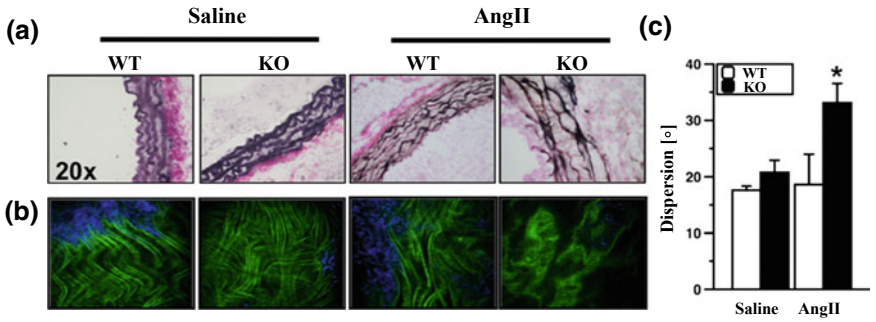

Fig. 19 Exemplar imaging analysis figure. Representative images of **a** elastin-stained aortic sections and **b** elastic lamellae by multiphoton fluorescence microscopy (green: elastin, blue: collagen; image width: 306 μm). **c** Quantification of the elastin signal from multiphoton data (1-sided Wilcoxon rank-sum test, $*P < 0.05$; $n = 4$ for each saline conditions and $n = 5$ for each experimental condition, AngII) based on the elastin fiber dispersion in the descending aorta. WT: wild-type, KO: transgenic model. Reproduced from [28]

is our opinion that representative imaging data should necessarily be presented, and can, if desired, be supplemented with more drastic examples. In any cases, the two should be differentiated explicitly.

6.1.2 Direct Metrics

The second step in image analysis is to choose a metric for quantification of a physical property of the tissue. The metric can directly capture the properties of interest. This is the case when stereological parameters are measured (number, length, surface area, and volume). Some ECM relevant examples are *i*) counting the number of elastic lamellae in the medial layer of an artery and *ii*) quantifying the volume occupied by collagen bundles in the adventitial layer of porcine arteries. Direct metrics are straightforward to interpret but can nonetheless be challenging to obtain. For instance, assessing the waviness of collagen bundles in adventitial collagen of porcine aorta by measuring the end-to-end distance and the contour length of individual fibers and then taking their ratio as the straightness parameter involves tedious manual tracing (Fig. 20a).

6.1.3 Indirect Metrics

An alternative solution is to select an indirect metric serving as a proxy for a physical parameter. Such indirect metrics are often more complex to interpret as they do not necessarily have a physical definition in the stereological sense and their variations can have multiple phenomenological origins. This complexity can lead to erroneous conclusion, and interpretations should be validated when needed. Figure 20b shows

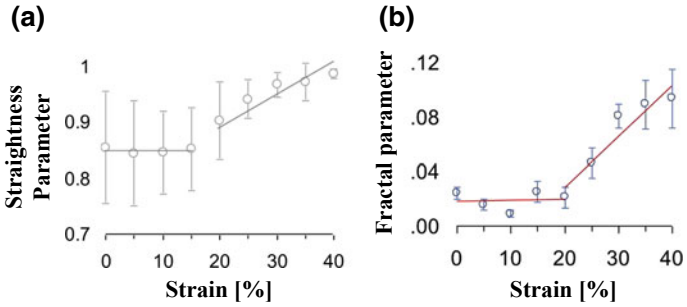

Fig. 20 Comparison between **a** a manual quantification of the waviness through direct length measurements and **b** automatic quantification with the proxy metric (fractal analysis) to characterize waviness in porcine adventitial collagen bundles during mechanical loading imaged with SHG. Reproduced with permission from [17]

the results of a fractal analysis as a function of strain of adventitial collagen from porcine aorta. For this specific case, the fractal analysis appears to be equivalent to the manual waviness analysis and can thus serve as a proxy for waviness (Fig. 20a was originally made to validate the interpretation of Fig. 20b). A clear advantage here is that the fractal analysis is computer automated. The absence of a need for manual inputs makes the analysis more consistent among users. Another important advantage is that the analysis can easily be adapted to other tissue types. Of course, when it is possible to automate the quantification of a direct metric, this option is preferable.

It was mentioned that indirect metrics variations can have a multitude of origins. To explain this fact, we will look again at the fractal analysis, but this time consider both medial collagen and elastin in porcine aorta during mechanical loading. The images reveal that waviness would have only a partial contribution in characterizing changes in the complex network of intertwined fibers (Fig. 1b) [17]. Yet, the fractal analysis revealed progressive changes in fiber organization and sequential recruitment of the different fiber families. It turns out that the fractal analysis metric is highly sensitive to any structural changes, including but not limited to waviness. It was therefore concluded that in the context of mechanical testing variations in the fractal number represent global changes in fiber engagement. Here, by making the interpretation more general, it also becomes more exact. This case also evidences another benefit of automated quantification of indirect metrics as they are a unique solution to quantitatively characterize tissue on which manual measurements cannot realistically be performed.

6.2 Dimensionality

Technical advances now make it possible to image 3D volumes in biological tissue with submicrometer spatial resolution. This capability should substantially circumvent the need to implement stereological methods of analysis of 2D images that inform on 3D parameters. However, 3D data requires analysis methods of the same dimensionality. The transition from 2D to 3D analysis is not trivial. Any manual measurements become much more time consuming. More importantly, automated methods that can perform essential tasks, such as following a fiber in multiple planes (for length measurements) or segmenting fiber bundles and lamellae for 3D reconstruction (for surface area and volume measurements), still need to be developed and their usage made robust for end-users.

In the meantime, a common approach in ECM imaging has consisted in compressing the 3D data to a 2D plane by performing intensity projections (Fig. 21). This approach allows one to use 2D analysis tools, which are extensively developed, for 3D data. The cost of this convenience is a loss of information. The point here is not to discourage the use of dimensional compression. After all, several important new observations about the ECM and its mechanical functions have been made with this simplistic strategy [17, 60]. However, it is important to be aware of the existing biases.

In projections, fiber length and waviness measurements are proxies for the actual fiber length and waviness in the 3D space; they are not stereological parameters. Lengths will appear shorter in projections if fibers do not reside in a single imaging plane. This bias is further pronounced during mechanical loading because as fibers are getting engaged, they will tend to rest increasingly within the imaging plane, i.e. the bias may change within a measurement. This applies for biaxial or uniaxial loading when the imaging plane contains one of the stretch axes. Another source of bias in characterizing fiber distribution originates from the use of the surface fraction, instead of volumetric fraction, occupied by a fiber group within a projected image as the weighting, or normalization, factor. Alleviating this bias is crucial as

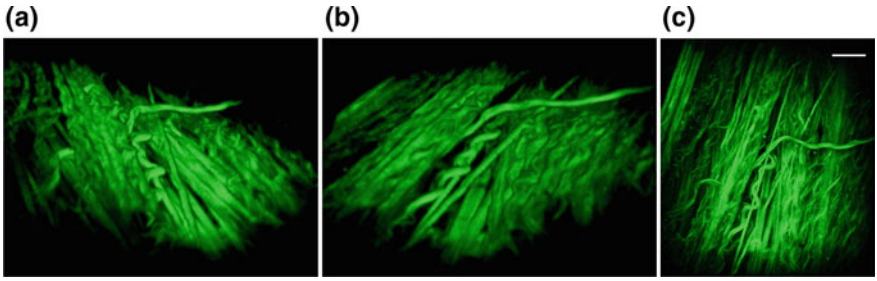

Fig. 21 Space compression. SHG signal from adventitial collagen in porcine aorta under mechanical loading shown as **a**, **b** 3D reconstructions from different angles and **c** a maximum intensity projection image along the axial dimension (scale bar: 50 μm)

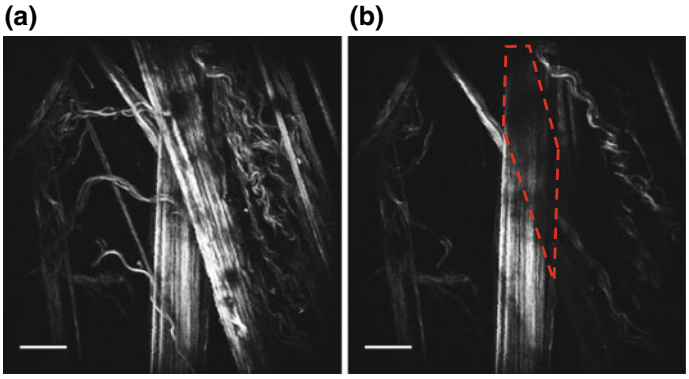

Fig. 22 Shadowing effect. SHG images from adventitial collagen in porcine aorta under mechanical loading. **a** Maximum intensity projection image (MIP) of the axial image stack. **b** MIP of the deeper half of the axial image stack. The red contour line indicates the shadowed area caused by the overlying collagen fibers. Scale bars: 50 μm

the distribution of fiber orientations is a central metric in mechanical modeling and to evaluate fiber recruitment [17, 49, 108, 109].

A common method to characterize the distribution of fiber orientation is the fast Fourier transform (FFT) analysis [17, 49, 106, 112]. During an FFT analysis [56], a projected image is divided into a matrix of small square regions. Then, each of these sub-regions is binarized independently before being Fourier transformed into the spatial frequency domain. Finally, the principal orientation is found for every sub-region through fitting an ellipse on the transform output. Typically, a histogram of the principal orientation (fiber angle) is generated to illustrate the distribution.

In addition to being susceptible to the bias caused by weighting, an optical shadowing effect further biases the results. The shadowing effect occurs when light propagating through a fiber bundle is altered to the extent the optical signal from any underlying structure is substantially degraded (Fig. 22). As a consequence, the results of FFT analysis are more heavily weighted toward bright and superficial structures. Several other limitations of the FFT analysis are discussed in the supplementary materials of [17].

To minimize the inherent bias associated with 2D image analysis, some effort has been made toward the development of 3D reconstruction tools for ECM images. Recently, the 3D surfaces of elastic lamellae in the mouse carotid artery were segmented (Fig. 23). Reconstruction is nevertheless only one of the necessary steps for a complete analysis. Due to the lack of quantification tools suitable to process 3D surfaces, the main discovery of this study, which provided the microstructural explanation for transmurally uniform lamellar stretching through a transmural gradient in lamellar unfolding, was still obtained from 2D circumferential cross-sections (but without dimensional compression) [107].

The distance between elastic lamellae was a key parameter in the above study (Fig. 23). A possible unbiased stereological strategy to quantify this parameter would

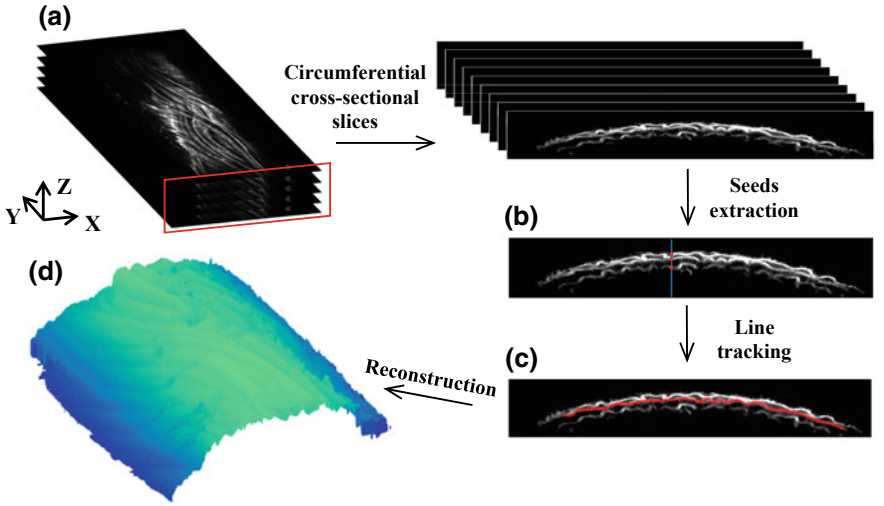

Fig. 23 3D image reconstruction. **a** The axial image stack images (TPEF from elastin in murine carotid arteries) are resliced before applying an algorithm to reconstruct the lamellar layers, which primarily involved **b** extraction of seed points and **c** line tracking from the seed points. **d** Reconstructed 3D elastic lamella. Reproduced with permission from [107]

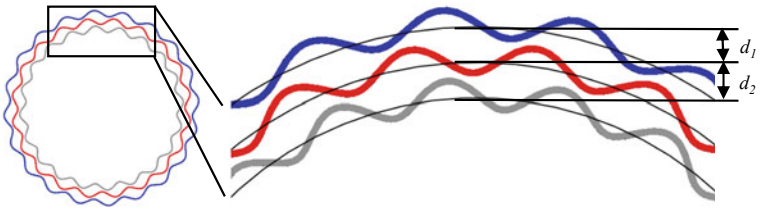

Fig. 24 Cylindrical geometry. Schematic of concentric elastic lamellar layers in the arterial wall. Assuming a cylindrical geometry substantially simplifies the evaluation of the interlamellar distances (d_i). Adapted from [107]

have been to evaluate the volumes between two lamella and to divide this value by the surface area corrected for curvature. The last step adds quite a lot of complexity, but this approach would ensure that no geometrical assumptions are made in the analysis and its outcome is hence unbiased. A way to simplify the quantification of interlamellar distances is to assume that the tissue possesses a cylindrical symmetry. Indeed, fitting circular segments onto lamellar profiles in circumferential cross-section was amply sufficient to measure precisely the distance between layers (Fig. 24). Selecting a geometry to which the biological samples are never a perfect match will cause bias. Nonetheless, this choice can be suitable when model-free stereological approaches are too complex for implementation.

6.3 Optics and Image Analysis

The optical system can also impact the quantitative analysis. Firstly, length estimates are dependent on the magnification, which is the scaling between the object and image planes [66]. This is true whether or not the imaging system is optical. This phenomenon is most commonly known as the *Coastline Paradox* and its explanation lies in fractal theory [58]. Length measurements acquired under different magnifications cannot therefore be compared.

Secondly, the mapping between the sample and the image is not always linear. The strength of the fluorescence signal is expected to be proportional to the concentration of fluorophores in the sample, for both one- and two- photon excitation. This relation is modulated by the depth dependence and other factors by which light is altered when propagating through biological tissue. More importantly, some contrast mechanisms scale nonlinearly with the number of scatterers or are coherent processes complexifying the mapping (e.g. the optical signal strength can be proportional to the square of the number of scatterers). The analysis of stereological parameters should be insensitive to the scaling (beyond how the scaling affect thresholding), but when using an indirect metric caution should be used.

Thirdly, optical images are a spatial convolution of the object, which occurs as light propagates through the instrument. This impulse response of optical systems is known as the *point spread function* (PSF) (Fig. 12a) and related to the spatial resolution (Fig. 3). For point-scanning systems, the axial extent is usually larger than the lateral one and this gives the PSF an ellipsoidal shape. The convolution will not affect distance measurements if they are performed between geometric centers of objects, but it will lead to a systematic overestimation of surfaces and volumes. If the PSF is known, a deconvolution can be numerically performed to limit the bias it introduces [87]. Even with deconvolution, one still doesn't get an infinite spatial frequency spectrum, but an improved image. It should also be noted that the PSF may vary as a function of depth, and sometimes lateral position, in biological tissue (see Sect. 4.2) and that applying deconvolution might not always be possible.

In summary, methods for image analysis should be validated, quantitative, and unbiased. All steps of image processing and analysis should be described when reporting results. It is also a good practice to take sufficient notes when performing manual measurements such that the analysis can be exactly repeated.

7 Conclusion and Future Directions

In this chapter, we presented fundamental concepts related to optical imaging, contrast mechanisms, imaging strategies, and image analysis. These concepts were positioned within the context of ECM imaging in an attempt to provide integrative guidelines for experimental design. We would like to reiterate that even if the discussion was focused on imaging for arteries, most, if not all, concepts addressed apply to other

types of biological tissues as well. Imaging data and statistical inferences can together provide powerful means for understanding complex multi-scale tissue mechanics. However, this can only be achieved by adopting an imaging method suitable for the length-scale of the structure of interest and also possessing the required signal specificity. Multiphoton microscopy is currently the optimal method for visualizing the microstructure of elastin and collagen ECM in intact tissue and we expect that this fundamental approach will yield many more discoveries in multiscale biomechanics in the years to come. The restricted imaging depth is the most important limitation of multiphoton microscopy to ECM imaging and advances on this front using a variety of strategies (e.g.: adaptive optics and optical clearing) would be highly beneficial through increased axial sampling. Increasing the imaging speed such that imaging in living animals is enabled would also constitute a substantial gain because it would then be possible to couple in vivo tissue deformation, ECM microstructure, and cellular dynamics in a unified experimental model.

Acknowledgements We would like to thank Matthew A. Mandelkern for proofreading. RT is very grateful to Prof. Charles P. Lin, who kindly provided a microscope over many years to perform mechanical ECM imaging studies. YZ gratefully acknowledges funding support from the National Institute of Health (2R01HL098028) and the National Science Foundation (CMMI 1463390 and CAREER 0954828).

References

1. Andersen, B.B., Korbo, L., Pakkenberg, B.: A quantitative study of the human cerebellum with unbiased stereological techniques. J. Comp. Neurol. **326**, 549–560 (1992)
2. Aviles-Espinosa, R., Andilla, J., Porcar-Guezenec, R., Olarte, O.E., Nieto, M., Levecq, X., Artigas, D., Loza-Alvarez, P.: Measurement and correction of in vivo sample aberrations employing a nonlinear guide-star in two-photon excited fluorescence microscopy. Biomed. Opt. Express. **2**, 3135–3149 (2011)
3. Bélanger, E., Turcotte, R., Daradich, A., Sadetsky, G., Gravel, P., Bachand, K., De Koninck, Y., Côté, D.C.: Maintaining polarization in polarimetric multiphoton microscopy. J. Biophotonics **8**, 884–888 (2015)
4. Booth, M.J.: Adaptive optical microscopy: the ongoing quest for a perfect image. Light Sci Appl. **3**, e165 (2014)
5. Booth, M.J., Neil, M., Wilson, T.: Aberration correction for confocal imaging in refractive-index-mismatched media. J. Microsc. **192**, 90–98 (1998)
6. Born, M., Wolf, E.: Principle of Optics. Cambridge University Press (1999)
7. Boudoux, C.: Fundamentals of Biomedical Optics. Blurb (2017)
8. Boulesteix, T., Pena, A.M., Pagès, N., Godeau, G., Sauviat, M.P., Beaurepaire, E., Schanne-Klein, M.C.: Micrometer scale ex vivo multiphoton imaging of unstained arterial wall structure. Cytometry A. **69**, 20–26 (2006)
9. Boyd, R.W.: Nonlinear Optics. Elsevier (2008)
10. Campagnola, P.: Second harmonic generation imaging microscopy: applications to diseases diagnostics. Anal. Chem. **83**, 3224–3231 (2011)
11. Campagnola, P.J., Loew, L.M.: Second-harmonic imaging microscopy for visualizing biomolecular arrays in cells, tissues and organisms. Nat. Biotechnol. **21**, 1356–1360 (2003)
12. Chen, F., Tillberg, P.W., Boyden, E.S.: Expansion microscopy. Science **347**, 543–548 (2015)

13. Chen, W.L., Li, T.H., Su, P.J., Chou, C.K., Fwu, P.T., Lin, S.J., Kim, D., Dong, C.Y.: Second harmonic generation χ tensor microscopy for tissue imaging. Appl. Phys. Lett. **94**, 183902 (2009)
14. Chen, X., Nadiarynkh, O., Plotnikov, S., Campagnola, P.J.: Second harmonic generation microscopy for quantitative analysis of collagen fibrillar structure. Nat. Protoc. **7**, 654–669 (2012)
15. Cheuk, B.L.Y., Cheng, S.W.K.: Expression of integrin α5β1 and the relationship to collagen and elastin content in human suprarenal and infrarenal aortas. Vasc Endovascular Surg. **39**, 245–251 (2005)
16. Chow, M.-J., Choi, M., Yun, S.H., Zhang, Y.: The effect of static stretch on elastin degradation in arteries. PLoS ONE **8**, e81951 (2013)
17. Chow, M.-J., Turcotte, R., Lin, C.P., Zhang, Y.: Arterial extracellular matrix: a mechanobiological study of the contributions and interactions of elastin and collagen. Biophys. J. **106**, 2684–2692 (2014)
18. Chu, S.-W., Chen, S.-Y., Chern, G.-W., Tsai, T.-H., Chen, Y.-C., Lin, B.-L., Sun, C.-K.: Studies of $\chi(2)/\chi(3)$ tensors in submicron-scaled bio-tissues by polarization harmonics optical microscopy. Biophys. J. **86**, 3914–3922 (2004)
19. Curatolo, A., Villiger, M., Lorenser, D., Wijesinghe, P., Fritz, A., Kennedy, B.F., Sampson, D.D.: Ultrahigh-resolution optical coherence elastography. Opt. Lett. **41**, 21–24 (2016)
20. Dan, D., Lei, M., Yao, B., Wang, W., Winterhalder, M., Zumbusch, A., Qi, Y., Xia, L., Yan, S., Yang, Y., Gao, P., Ye, T., Zhao, W.: DMD-based LED-illumination super-resolution and optical sectioning microscopy. Sci. Reports. **3**, 1116 (2013)
21. Davis, E.C.: Smooth muscle cell to elastic lamina connections in developing mouse aorta. Role in aortic medial organization. Lab. Invest. **68**, 89–99 (1993)
22. de Aguiar, H.B., Gasecka, P., Brasselet, S.: Quantitative analysis of light scattering in polarization-resolved nonlinear microscopy. Opt. Express **23**, 8960–8973 (2015)
23. Drobizhev, M., Makarov, N.S., Tillo, S.E., Hughes, T.E., Rebane, A.: Two-photon absorption properties of fluorescent proteins. Nat. Methods **8**, 393–399 (2011)
24. Duboisset, J., Rigneault, H., Brasselet, S.: Filtering of matter symmetry properties by circularly polarized nonlinear optics. Phys. Rev. A. **90**, 063827 (2014)
25. Empedocles, S.A., Neuhauser, R., Bawendi, M.G.: Three-dimensional orientation measurements of symmetric single chromophores using polarization microscopy. Nature **399**, 126–130 (1999)
26. Fata, B., Carruthers, C.A., Gibson, G., Watkins, S.C., Gottlieb, D., Mayer, J.E., Sacks, M.S.: Regional structural and biomechanical alterations of the ovine main pulmonary artery during postnatal growth. J. Biomech. Eng. **135**, 021022 (2013)
27. Fellgett, P.B., Linfoot, E.H.: On the assessment of optical images. Philos. Trans. R. Soc. Lond. **247**, 369–407 (1955)
28. Fry, J.L., Shiraishi, Y., Turcotte, R., Yu, X., Gao, Y.Z., Akiki, R., Bachschmid, M., Zhang, Y., Morgan, K.G., Cohen, R.A., Seta, F.: Vascular Smooth Muscle Sirtuin-1 Protects Against Aortic Dissection During Angiotensin II-Induced Hypertension. J. Am. Heart Assoc. **4**, e002384 (2015)
29. García-Herrera, C.M., Celentano, D.J., Cruchaga, M.A., Rojo, F.J., Atienza, J.M., Guinea, G.V., Goicolea, J.M.: Mechanical characterisation of the human thoracic descending aorta: Experiments and modelling. Comput. Methods Biomech. Biomed. Engin. **15**, 185–193 (2012)
30. Gerson, C.J., Goldstein, S., Heacox, A.E.: Retained structural integrity of collagen and elastin within cryopreserved human heart valve tissue as detected by two-photon laser scanning confocal microscopy. Cryobiology **59**, 171–179 (2009)
31. Gundersen, H.J.G., Jensen, E.B.: The efficiency of systematic sampling in stereology and its prediction. J. Microsc. **147**, 229–263 (1987)
32. Gusachenko, I., Latour, G., Schanne-Klein, M.-C.: Polarization-resolved Second Harmonic microscopy in anisotropic thick tissues. Opt. Express **18**, 19339–19352 (2010)
33. Gusachenko, I., Schanne-Klein, M.-C.: Numerical simulation of polarization-resolved second-harmonic microscopy in birefringent media. Phys. Rev. A **88**, 101–115 (2013)

34. Gusachenko, I., Tran, V., Goulam Houssen, Y., Allain, J.-M., Schanne-Klein, M.-C.: Polarization-resolved second-harmonic generation in tendon upon mechanical stretching. Biophys. J. **102**, 2220–2229 (2012)
35. Halloran, B.G., Davis, V.A., McManus, B.M., Lynch, T.G., Baxter, B.T.: Localization of aortic disease is associated with intrisinc differences in aortic structure. J. Surg. Res. **59**, 17–22 (1995)
36. Harkness, M.L.R., Harkness, R.D., McDonald, D.A.: The collagen and elastin content of the arterial wall in the dog. Proc. R. Soc. Lond., B, Biol. Sci. **146**, 541–551 (1957)
37. Hecht, E.: Optique (fr). Pearson (2005)
38. Hill, M.R., Duan, X., Gibson, G.A., Watkins, S., Robertson, A.M.: A theoretical and non-destructive experimental approach for direct inclusion of measured collagen orientation and recruitment into mechanical models of the artery wall. J. Biomech. **45**, 762–771 (2012)
39. Hill-Eubanks, D.C., Werner, M.E., Heppner, T.J., Nelson, M.T.: Calcium signaling in smooth muscle. Cold Spring Harb. Perspect. Biol. **3**, a004549 (2011)
40. Holzapfel, G.A., Gasser, T.C., Ogden, R.W.: A new constitutive framework for arterial wall mechanics and a comparative study of material models. J. Elast. **61**, 1–48 (2000)
41. Hovhannisyan, V., Ghazaryan, A., Chen, Y.-F., Chen, S.-J., Dong, C.Y.: Photophysical mechanisms of collagen modification by 80 MHz femtosecond laser. Opt. Express **18**, 24037–24047 (2010)
42. Hunziker, E.B., Cruz-Orive, L.M.: Consistent and efficient delineation of reference spaces for light microscopical stereology using a laser microbeam system. J. Microsc. **142**, 95–99 (1986)
43. Jacques, S.L.: Optical properties of biological tissues: a review. Phys. Med. Biol. **58**, R37–61 (2013)
44. Ji, N.: Adaptive optical fluorescence microscopy. Nat. Methods **14**, 374–380 (2017)
45. Kennedy, B.F., McLaughlin, R.A., Kennedy, K.M., Chin, L., Curatolo, A., Tien, A., Latham, B., Saunders, C.M., Sampson, D.D.: Optical coherence micro-elastography: mechanical-contrast imaging of tissue microstructure. Biomed. Opt. Express. **5**, 2113–2124 (2014)
46. Kim, J., Hong, J.-W., Baek, S.: Longitudinal differences in the mechanical properties of the thoracic aorta depend on circumferential regions. J Biomed Mater Res A. **101**, 1525–1529 (2013)
47. Kobat, D., Durst, M.E., Nishimura, N., Wong, A.W., Schaffer, C.B., Xu, C.: Deep tissue multiphoton microscopy using longer wavelength excitation. Opt. Express **17**, 13354–13364 (2009)
48. König, K., So, P.T., Mantulin, W.W., Gratton, E.: Cellular response to near-infrared femtosecond laser pulses in two-photon microscopes. Opt. Lett. **22**, 135–136 (1997)
49. Krasny, W., Morin, C., Magoariec, H., Avril, S.: A comprehensive study of layer-specific morphological changes in the microstructure of carotid arteries under uniaxial load. Acta Biomater. **57**, 342–351 (2017)
50. Kwok, S.J.J., Kuznetsov, I.A., Kim, M., Choi, M., Scarcelli, G., Yun, S.H.: Selective two-photon collagen crosslinking in situ measured by Brillouin microscopy. Optica. **3**, 469–472 (2016)
51. Labrosse, M.R., Beller, C.J., Mesana, T., Veinot, J.P.: Mechanical behavior of human aortas: Experiments, material constants and 3-D finite element modeling including residual stress. J. Biomech. **42**, 996–1004 (2009)
52. Le Floc'h, V., Brasselet, S., Roch, J.-F., Zyss, J.: Monitoring of orientation in molecular ensembles by polarization sensitive nonlinear microscopy. J. Phys. Chem. B. **107**, 12403–12410 (2003)
53. Lee, K.-W., Stolz, D.B., Wang, Y.: Substantial expression of mature elastin in arterial constructs. Proc. Natl. Acad. Sci. U.S.A. **108**, 2705–2710 (2011)
54. Lim, D., Chu, K.K., Mertz, J.: Wide-field fluorescence sectioning with hybrid speckle and uniform-illumination microscopy. Opt. Lett. **33**, 1819–1821 (2008)
55. Lim, D., Ford, T.N., Chu, K.K., Mertz, J.: Optically sectioned in vivo imaging with speckle illumination HiLo microscopy. J. Biomed. Opt. **16**, 016014 (2011)

56. Liu, Z.Q.: Scale space approach to directional analysis of images. Appl. Opt. **30**, 1369–1373 (1991)
57. Lu-Walther, H.-W., Kielhorn, M., Förster, R., Jost, A., Wicker, K., Heintzmann, R.: fastSIM: a practical implementation of fast structured illumination microscopy. Methods Appl. Fluoresc. **3**, 014001 (2015)
58. Mandelbrot, B.: How long is the coast of britain? Statistical self-similarity and fractional dimension. Science. **156**, 636–638 (1967)
59. Matsumoto, N., Konno, A., Inoue, T., Okazaki, S.: Aberration correction considering curved sample surface shape for non-contact two-photon excitation microscopy with spatial light modulator. Sci. Rep. **8**, 9252 (2018)
60. Mattson, J.M., Turcotte, R., Zhang, Y.: Glycosaminoglycans contribute to extracellular matrix fiber recruitment and arterial wall mechanics. Biomech. Model. Mechanobiol. **16**, 213–225 (2017)
61. Mattson, J.M., Wang, Y., Zhang, Y.: Contributions of glycosaminoglycans to collagen fiber recruitment in constitutive modeling of arterial mechanics. J. Biomech. **82**, 211–219 (2019)
62. Mazumder, N., Deka, G., Wu, W.-W., Gogoi, A., Zhuo, G.-Y., Kao, F.-J.: Polarization resolved second harmonic microscopy. Methods **128**, 105–118 (2017)
63. Mertz, J.: Introduction to optical microscopy. Roberts and Company Publishers (2010).
64. Mertz, J.: Optical sectioning microscopy with planar or structured illumination. Nat. Methods **8**, 811–819 (2011)
65. Mondal, P.P.: Temporal resolution in fluorescence imaging. Front Mol Biosci. **1**, 11 (2014)
66. Mouton, P.R.: Principles and practices of unbiased stereology. The Johns Hopkins University Press (2002)
67. Müllenbroich, C.M., McGhee, E.J., Wright, A.J., Anderson, K.I., Mathieson, K.: Strategies to overcome photobleaching in algorithm-based adaptive optics for nonlinear in-vivo imaging. J. Biomed. Opt. **19**, 16021 (2014)
68. Neil, M., Juskaitis, R., Wilson, T.: Method of obtaining optical sectioning by using structured light in a conventional microscope. Opt. Lett. **22**, 1905–1907 (1997)
69. Ostroverkhov, V., Singer, K.D., Petschek, R.G.: Second-harmonic generation in nonpolar chiral materials: relationship between molecular and macroscopic properties. J. Opt. Soc. Am. B. **18**, 1858–1865 (2001)
70. Pawley, J.: Handbook of Biological Confocal Microscopy. Springer (2006)
71. Plotnikov, S., Juneja, V., Isaacson, A.B., Mohler, W.A., Campagnola, P.J.: Optical clearing for improved contrast in second harmonic generation imaging of skeletal muscle. Biophys. J. **90**, 328–339 (2006)
72. Ranjit, S., Dvornikov, A., Stakic, M., Hong, S.-H., Levi, M., Evans, R.M., Gratton, E.: Imaging fibrosis and separating collagens using second harmonic generation and phasor approach to fluorescence lifetime imaging. Sci. Rep. **5**, 13378 (2015)
73. Raub, C.B., Suresh, V., Krasieva, T., Lyubovitsky, J., Mih, J.D., Putnam, A.J., Tromberg, B.J., George, S.C.: Noninvasive assessment of collagen gel microstructure and mechanics using multiphoton microscopy. Biophys. J. **92**, 2212–2222 (2007)
74. Roccabianca, S., Figueroa, C.A., Tellides, G., Humphrey, J.D.: Quantification of regional differences in aortic stiffness in the aging human. J. Mech. Behav. Biomed. Mater. **29**, 618–634 (2014)
75. Rogowska, J., Patel, N., Plummer, S., Brezinski, M.E.: Quantitative optical coherence tomographic elastography: method for assessing arterial mechanical properties. Br. J. Radiol. **79**, 707–711 (2006)
76. Rouleau, L., Tremblay, D., Cartier, R., Mongrain, R., Leask, R.L.: Regional variations in canine descending aortic tissue mechanical properties change with formalin fixation. Cardiovasc. Pathol. **21**, 390–397 (2012)
77. Russ, J.C., Dehoff, R.T., Deh: Practical stereology. Springer (2012)
78. Sahl, S.J., Hell, S.W., Jakobs, S.: Fluorescence nanoscopy in cell biology. Nat. Rev. Mol. Cell Biol. **18**, 685–701 (2017)

79. Scarcelli, G., Yun, S.H.: Confocal Brillouin microscopy for three-dimensional mechanical imaging. Nat. Photonics **2**, 39–43 (2007)
80. Schenke-Layland, K.: Non-invasive multiphoton imaging of extracellular matrix structures. J. Biophotonics **1**, 451–462 (2008)
81. Smith, A.M., Mancini, M.C., Nie, S.: Bioimaging: second window for in vivo imaging. Nat. Nanotechnol. **4**, 710–711 (2009)
82. Sokolis, D.P.: Passive mechanical properties and structure of the aorta: segmental analysis. Acta Physiol. **190**, 277–289 (2007)
83. Sokolis, D.P., Boudoulas, H., Kavantzas, N.G., Kostomitsopoulos, N., Agapitos, E.V., Karayannacos, P.E.: A morphometric study of the structural characteristics of the aorta in pigs using an image analysis method. Anat. Histol. Embryol. **31**, 21–30 (2002)
84. Song, L., Lu-Walther, H.-W., Förster, R., Jost, A., Kielhorn, M., Zhou, J., Heintzmann, R.: Fast structured illumination microscopy using rolling shutter cameras. Meas. Sci. Technol. **27**, 055401 (2016)
85. Stoller, P., Reiser, K.M., Celliers, P.M., Rubenchik, A.M.: Polarization-modulated second harmonic generation in collagen. Biophys. J. **82**, 3330–3342 (2002)
86. Sun, Y., Sun, Y., Stephens, D., Xie, H., Phipps, J., Saroufeem, R., Southard, J., Elson, D.S., Marcu, L.: Dynamic tissue analysis using time- and wavelength-resolved fluorescence spectroscopy for atherosclerosis diagnosis. Opt. Express **19**, 3890–3901 (2011)
87. Swedlow, J.R., Sedat, J.W., Agard, D.A.: Deconvolution in optical microscopy. In: Deconvolution of images and spectra. pp. 284–309, Orlando, FL, USA (1997)
88. Teulon, C., Gusachenko, I., Latour, G., Schanne-Klein, M.-C.: Theoretical, numerical and experimental study of geometrical parameters that affect anisotropy measurements in polarization-resolved SHG microscopy. Opt. Express **23**, 9313–9328 (2015)
89. Tuer, A.E., Akens, M.K., Krouglov, S., Sandkuijl, D., Wilson, B.C., Whyne, C.M., Barzda, V.: Hierarchical Model of fibrillar collagen organization for interpreting the second-order susceptibility tensors in biological tissue. Biophys. J. **103**, 2093–2105 (2012)
90. Turcotte, R., Liang, Y., Ji, N.: Adaptive optical versus spherical aberration corrections for in vivo brain imaging. Biomed. Opt. Express. **8**, 3891–3902 (2017)
91. Turcotte, R., Mattson, J.M., Wu, J.W., Zhang, Y., Lin, C.P.: Molecular order of arterial collagen using circular polarization second-harmonic generation imaging. Biophys. J. **110**, 530–533 (2016)
92. Tønnesen, J., Inavalli, V.V.G.K., Nägerl, U.V.: Super-resolution imaging of the extracellular space in living brain tissue. Cell **172**, 1108–1121 (2018)
93. Veilleux, I., Spencer, J.A., Bliss, D.P., Côté, D., Lin, C.P.: In vivo cell tracking with video rate multimodality laser scanning microscopy. IEEE J. Sel. Top. Quantum Electron. 14, 10–18 (2008)
94. Wagnieres, G.A., Star, W.M., Wilson, B.C.: In vivo fluorescence spectroscopy and imaging for oncological applications. Photochem. Photobiol. **68**, 603–632 (1998)
95. Wan, W., Dixon, J.B., Gleason, R.L.: Constitutive modeling of mouse carotid arteries using experimentally measured microstructural parameters. Biophys. J. **102**, 2916–2925 (2012)
96. Wang, K., Milkie, D.E., Saxena, A., Engerer, P., Misgeld, T., Bronner, M.E., Mumm, J., Betzig, E.: Rapid adaptive optical recovery of optimal resolution over large volumes. Nat. Methods **11**, 625–628 (2014)
97. Wang, K., Sun, W., Richie, C.T., Harvey, B.K., Betzig, E., Ji, N.: Direct wavefront sensing for high-resolution in vivo imaging in scattering tissue. Nat. Commun. **6**, 7276 (2015)
98. Wang, Y., Li, H., Zhang, Y.: Understanding the viscoelastic behavior of arterial elastin in glucose via relaxation time distribution spectrum. J. Mech. Behav. Biomed. Mater. **77**, 634–641 (2018)
99. Wang, Y., Zeinali-Davarani, S., Zhang, Y.: Arterial mechanics considering the structural and mechanical contributions of ECM constituents. J. Biomech. **49**, 2358–2365 (2016)
100. Webb, W.W., Xu, C.: Measurement of two-photon excitation cross sections of molecular fluorophores with data from 690 to 1050 nm. J. Opt. Soc. Am. B. **13**, 481–491 (1996)

101. West, M.J.: Basic Stereology for Biologists and Neuroscientists. Cold Spring Harbor Press (2012)
102. West, M.J., Gundersen, H.J.G.: Unbiased Stereological Estimation of the number of neurons in the human hippocampus. J. Comp. Neurol. **296**, 1–22 (1990)
103. Wicker, K., Heintzmann, R.: Resolving a misconception about structured illumination. Nat. Photonics **8**, 342–344 (2014)
104. Wicker, K., Mandula, O., Best, G., Fiolka, R., Heintzmann, R.: Phase optimisation for structured illumination microscopy. Opt. Express **21**, 2032–2049 (2013)
105. Wolinsky, H., Glagov, S.: Comparison of abdominal and thoracic aortic medial structure in mammals. Circ. Res. **25**, 677–686 (1969)
106. Wu, S., Li, H., Yang, H., Zhang, X., Li, Z., Xu, S.: Quantitative analysis on collagen morphology in aging skin based on multiphoton microscopy. J. Biomed. Opt. **16**, 040502 (2011)
107. Yu, X., Turcotte, R., Seta, F., Zhang, Y.: Micromechanics of elastic lamellae: unravelling the role of structural inhomogeneity in multi-scale arterial mechanics. J. R. Soc. Interface. **15**, 20180492 (2018)
108. Yu, X., Wang, Y., Zhang, Y.: Transmural variation in elastin fiber orientation distribution in the arterial wall. J. Mech. Behav. Biomed. Mater. **77**, 745–753 (2018)
109. Zeinali-Davarani, S., Chow, M.-J., Turcotte, R., Zhang, Y.: Characterization of biaxial mechanical behavior of porcine aorta under gradual elastin degradation. Ann Biomed Eng. **41**, 1528–1538 (2013)
110. Zeinali-Davarani, S., Wang, Y., Chow, M.-J., Turcotte, R., Zhang, Y.: Contribution of collagen fiber undulation to regional biomechanical properties along porcine thoracic aorta. J. Biomech. Eng. **137**, 051001 (2015)
111. Zhao, H.L., Zhang, C.P., Zhu, H., Jiang, Y.F., Fu, X.B.: Autofluorescence of collagen fibres in scar. Skin. Res. Technol. **23**, 588–592 (2017)
112. Zhu, X., Zhuo, S., Zheng, L., Lu, K., Jiang, X., Chen, J., Lin, B.: Quantified characterization of human cutaneous normal scar using multiphoton microscopy. J. Biophotonics. **3**, 108–116 (2010)
113. Zipfel, W.R., Williams, R.M., Christie, R., Nikitin, A.Y., Hyman, B.T., Webb, W.W.: Live tissue intrinsic emission microscopy using multiphoton-excited native fluorescence and second harmonic generation. Proc. Natl. Acad. Sci. USA **100**, 7075–7080 (2003)
114. Zipfel, W.R., Williams, R.M., Webb, W.W.: Nonlinear magic: multiphoton microscopy in the biosciences. Nat. Biotechnol. **21**, 1369–1377 (2003)
115. Zou, Y., Zhang, Y.: An experimental and theoretical study on the anisotropy of elastin network. Ann. Biomed. Eng. **37**, 1572–1583 (2009)
116. Zoumi, A., Lu, X., Kassab, G.S., Tromberg, B.J.: Imaging coronary artery microstructure using second-harmonic and two-photon fluorescence microscopy. Biophys. J. **87**, 2778–2786 (2004)
117. Zoumi, A., Yeh, A., Tromberg, B.J.: Imaging cells and extracellular matrix in vivo by using second-harmonic generation and two-photon excited fluorescence. Proc. Natl. Acad. Sci. USA **99**, 11014–11019 (2002)